# Secondary flow in sharp open-channel bends

## By K. BLANCKAERT[1] and H. J. de VRIEND[2]

[1]Lab. d'Hydraulique Environnementale, Ecole Polytechnique Fédérale, CH-1015 Lausanne, Switzerland
[2]Delft University of Technology, POB 5048, 2600 GA Delft, The Netherlands

Secondary currents are a characteristic feature of flow in open-channel bends. Besides the classical helical motion (centre-region cell), a weaker and smaller counter-rotating circulation cell (outer-bank cell) is often observed near the outer bank, which is believed to play an important role in bank erosion processes. The mechanisms underlying the circulation cells, especially the outer-bank cell, are still poorly understood, and their numerical simulation still poses problems, not least due to lack of detailed experimental data. The research reported herein provides detailed experimental data on both circulation cells in an open-channel bend such as found in nature. Furthermore, the underlying dynamics are investigated by simultaneously analysing the vorticity equation and the kinetic energy transfer between the mean flow and the turbulence. This shows that turbulence plays a minor role in the generation of the centre-region cell, which is mainly due to the centrifugal force. By accounting for the feedback between the downstream velocity profile and the centre-region cell, a strongly simplified vorticity balance is shown to yield accurate predictions of the velocities in the centre region. For strong curvatures, however, a fully three-dimensional flow description is required. Due to the non-monotonic velocity profiles, the centrifugal force favours the outer-bank cell. Moreover, terms related to the anisotropy of the cross-stream turbulence, induced by boundary proximity, are of the same order of magnitude and mainly enhance the outer-bank cell. Both mechanisms strengthen each other. The occurrence of the outer-bank cell is shown to be not just due to flow instability, like in the case of curved laminar flow, but also to kinetic energy input from turbulence.

## 1. Introduction

Curved open-channel flow is characterized by the existence of cross-stream circulation cells (secondary flow). By advecting flow momentum, these determine the spatial distributions of the velocities and the boundary shear stresses (Blanckaert & Graf 2004), and thereby shape the topography in the case of a mobile bottom.

Besides the 'classical' helical motion (called hereafter the centre-region cell) that covers a large part of the cross-section (called hereafter the centre region), a weaker counter-rotating cell is often observed near the outer bank. Although relatively small and weak, this outer-bank cell is important, as it tends to protect steep outer banks from erosion (Christensen, Gislason & Fredsoe 1999; Blanckaert & Graf 2004). Figure 1 illustrates both circulation cells in a reach of an open-channel bend.

Detailed experiments on these two circulation cells are scarce (Booij & Tukker 1996; Blanckaert & Graf 2001; Blanckaert 2002*a*, *b*; Booij 2003), because they require accurate high-resolution measurements of the transverse and vertical velocity components on a fine grid. Many experimental investigations so far have provided
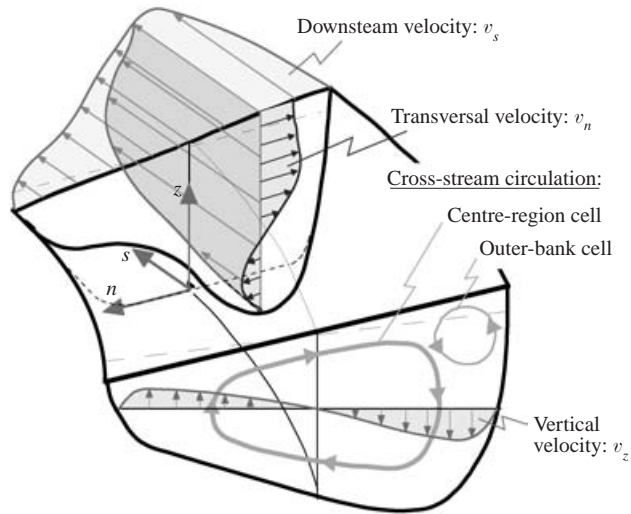
FIGURE 1. Definition sketch of curved open-channel flow and cross-stream circulation.

data with a relatively low accuracy on a relatively coarse grid (see Blanckaert & Graf 2001). This explains why, in spite of the fact that the occurrence of the second cell was reported in the literature long ago (e.g. Mockmore 1943), studies usually concentrate on the centre-region cell far from the banks.

The mechanisms underlying the two circulation cells are revealed by the downstream vorticity balance, in which the centrifugal force and the cross-stream turbulent stresses play a dominant role. So far, the experimental confirmation of this observation has been hampered by the scarcity of measured data on these cross-stream turbulent stresses.

The centre-region cell is usually explained in terms of the local imbalance between the driving centrifugal force and the transverse pressure gradient (e.g. Rozovskii 1957). Turbulence is known to be important to the generation of the outer-bank cell. Yet, there is little insight available into the dynamics of the turbulence in the vicinity of that cell, and even the conditions of occurrence of the outer-bank cell are almost unknown.

The experimental research presented herein aims at obtaining a more detailed picture of the double-cell pattern in an open-channel bend such as found in nature, so as to gain insight into its dynamics and especially into the role of turbulence, and to find guidance for numerical modelling. In order to clarify the role of turbulence, we simultaneously analyse the vorticity equation and the kinetic energy transfer between mean flow and turbulence. The experimental data are derived from simultaneous high-resolution measurements of the three velocity components on a fine grid in one cross-section of a bend in a laboratory flume. This makes it possible to evaluate all three mean velocity components, as well as all turbulent stress components. Based on these results, the relevant terms in the vorticity equation and the kinetic energy transfer between the mean flow and the turbulence can be evaluated.

In the first part of this paper, a theoretical framework of the analysis is given and the current state of knowledge on the cross-stream circulation is reviewed. The importance of considering the kinetic energy transfer between mean flow and turbulence is shown. Subsequently, the experiment is presented and the mechanisms underlying the two circulation cells are analysed on the basis of the experimental

data and focusing on the downstream vorticity balance and the exchange of kinetic energy. Special attention is paid to the implications for numerical modelling.

## 2. The downstream vorticity equation

A cylindrical coordinate system is adopted, with the curvilinear $s$-axis pointing downstream along the channel axis, the transversal $n$-axis pointing to the left and the vertical $z$-axis pointing the upward from the horizontal $(s, n)$-plane (also see figures 1 and 2). The transformation of the flow equations from a Cartesian to a cylindrical coordinate system is given by Batchelor (1970, p. 598).

The cross-stream motion, $(v_n, v_z)$, is governed by the transverse and vertical momentum equations for incompressible flow (Schlichting & Gersten 2000):

$$\frac{\partial v_n}{\partial t} = -\left( \frac{1}{1+n/R} v_s \frac{\partial v_n}{\partial s} + v_n \frac{\partial v_n}{\partial n} + v_z \frac{\partial v_n}{\partial z} - \frac{1}{1+n/R} \frac{v_s^2}{R} \right)$$
$$- \frac{1}{\rho} \frac{\partial p}{\partial n} - \left( \frac{1}{1+n/R} \frac{\partial \overline{v_s' v_n'}}{\partial s} + \frac{\partial \overline{v_n'^2}}{\partial n} + \frac{\partial \overline{v_n' v_z'}}{\partial z} + \frac{1}{1+n/R} \frac{\overline{v_n'^2} - \overline{v_s'^2}}{R} \right)$$
$$+ \nu \left( \nabla^2 v_n - \frac{1}{(1+n/R)^2} \frac{1}{R} \frac{\partial v_s}{\partial s} - \frac{1}{1+n/R} \frac{\partial}{\partial s} \left( \frac{1}{1+n/R} \frac{1}{R} v_s \right) \right.$$
$$\left. - \frac{1}{(1+n/R)^2} \frac{1}{R^2} v_n \right), \tag{1}$$

$$\frac{\partial v_z}{\partial t} = -\left( \frac{1}{1+n/R} v_s \frac{\partial v_z}{\partial s} + v_n \frac{\partial v_z}{\partial n} + v_z \frac{\partial v_z}{\partial z} \right)$$
$$- g - \frac{1}{\rho} \frac{\partial p}{\partial z} - \left( \frac{1}{1+n/R} \frac{\partial \overline{v_s' v_z'}}{\partial s} + \frac{\partial \overline{v_n' v_z'}}{\partial n} + \frac{\partial \overline{v_z'^2}}{\partial z} + \frac{1}{1+n/R} \frac{\overline{v_n' v_z'}}{R} \right) + \nu \nabla^2 v_z, \tag{2}$$

in which $(1+n/R)$ is a metric factor accounting for the divergence of the $n$-coordinate lines, $R$ being the radius of curvature of the channel axis; $p$ is the pressure; $t$ is time; $g$ is the gravitational acceleration; $\vec{v} = (v_s, v_n, v_z)$ and $\vec{v}' = (v_s', v_n', v_z')$ are the mean and fluctuating velocity components; $-\rho \overline{v_j' v_k'}$ ($j, k = s, n, z$) are the turbulent stresses; $\nu$ is the molecular kinematic viscosity; $\nabla^2$ is the Laplace operator.

The transverse momentum equation (1) is dominated by the centrifugal-force and pressure-gradient terms, which nearly balance each other. The vertical momentum equation (2) is dominated by the hydrostatic balance, $g + \rho^{-1} \partial p / \partial z \approx 0$. Thus these equations do not clearly reveal the dynamics of the cross-stream motion. For clarity, a distinction will be made between the translatory and the circulatory parts of the cross-stream motion, which Bradshaw (1987) names cross-flow and identifiable downstream vortices, respectively. The translatory part, which is mainly pressure-induced, will not be considered herein. The circulatory part, which is independent of the pressure field, is represented by the downstream component of the vorticity vector

$$\omega_s = \frac{\partial v_z}{\partial n} - \frac{\partial v_n}{\partial z}. \tag{3}$$

Thus the cross-stream circulation is represented by a scalar, instead of a vector field. The downstream vorticity balance provides a good basis for analysis. The corresponding equation is obtained by cross-differentiation of equations (1) and (2),

thus eliminating the pressure:

$$\frac{\partial \omega_s}{\partial t} = -\left(\frac{1}{1+n/R}v_s\frac{\partial \omega_s}{\partial s} + v_n\frac{\partial \omega_s}{\partial n} + v_z\frac{\partial \omega_s}{\partial z}\right) + \frac{1}{1+n/R}\omega_s\frac{\partial v_s}{\partial s}$$

$$+ \left[\omega_n\frac{\partial v_s}{\partial n} + \omega_z\frac{\partial v_s}{\partial z} + \frac{1}{1+n/R}\frac{v_n\omega_s}{R} - \frac{1}{1+n/R}\frac{v_s\omega_n}{R}\right] - \frac{1}{1+n/R}\frac{\partial}{\partial z}\left(\frac{\overline{v_s'^2}}{R}\right)$$

$$+ \frac{\partial^2}{\partial z\partial n}\left(\overline{v_n'^2} - \overline{v_z'^2}\right) + \frac{1}{1+n/R}\frac{1}{R}\frac{\partial \overline{v_n'^2}}{\partial z}$$

$$+ \left\{\frac{1}{1+n/R}\frac{\partial^2}{\partial z^2} - \frac{\partial}{\partial n}\left(\frac{1}{1+n/R}\frac{\partial}{\partial n}\right)\right\}\left[(1+n/R)\overline{v_n'v_z'}\right]$$

$$+ \frac{\partial}{\partial z}\left(\frac{1}{1+n/R}\frac{\partial \overline{v_s'v_n'}}{\partial s}\right) - \frac{\partial}{\partial n}\left(\frac{1}{1+n/R}\frac{\partial \overline{v_s'v_z'}}{\partial s}\right)$$

$$+ \nu\left(\nabla^2\omega_s + \frac{2}{(1+n/R)^2}\frac{1}{R}\frac{\partial \omega_n}{\partial s} - \frac{1}{(1+n/R)^2}\frac{1}{R^2}\omega_s\right), \tag{4}$$

in which the *n*- and *z*-components of the vorticity vector are defined by

$$\omega_n = \frac{\partial v_s}{\partial z} - \frac{1}{1+n/R}\frac{\partial v_z}{\partial s}, \quad \omega_z = \frac{1}{1+n/R}\frac{\partial v_n}{\partial s} - \frac{\partial v_s}{\partial n} - \frac{1}{1+n/R}\frac{v_s}{R}. \tag{5}$$

Without pretending mathematical rigour, this equation can be interpreted as follows in physical terms (e.g. Perkins 1970; Demuren & Rodi 1984; Bradshaw 1987; Nezu & Nakagawa 1993):

(i) The terms $v_n\partial\omega_s/\partial n + v_z\partial\omega_s/\partial z$ in the first line represent the advective transport of downstream vorticity by the cross-stream motion ($v_n$, $v_z$). This mechanism does not generate or dissipate $\omega_s$, but just redistributes it over the cross-section.

(ii) The $\omega_s\partial v_s/\partial s$-term in the first line represents amplification of $\omega_s$ due to vortex stretching.

(iii) The terms in square brackets in the second line represent skewing-induced vorticity redistribution by quasi-inviscid deflection of existing mean vorticity $\bar{\omega}(\omega_s, \omega_n, \omega_z)$. Skewing-induced vorticity corresponds to Prandtl's circulation of the first kind (Prandtl 1942, pp. 130–134). By substitution of the definitions (3) and (5), these terms can be transformed into

$$-\frac{1}{1+n/R}\frac{\partial}{\partial z}\left(\frac{v_s^2}{R}\right) + \frac{1}{1+n/R}\frac{v_n\omega_s}{R} + \left[\frac{1}{1+n/R}\frac{\partial v_n}{\partial s}\frac{\partial v_s}{\partial z} - \frac{\partial v_z}{\partial s}\frac{\partial}{\partial n}\left(\frac{1}{1+n/R}v_s\right)\right], \tag{6}$$

showing terms accounting for downstream non-uniformities (the $\partial/\partial s$-terms in square brackets), a curvature-induced term with $v_n\omega_s/R$, and a term associated with the centrifugal force, $-v_s^2/R$. The latter term shows that the centrifugal force is a source of skewing-induced vorticity.

(iv) The last term in the second line of the equation is a turbulence-related centrifugal force term.

(v) The third and fourth lines represent the influence of the cross-stream turbulent stress components on the vorticity field. Globally, vorticity is dissipated by these turbulent stresses. In certain regions of the flow domain, however, these terms represent generation of mean vorticity (see below). Turbulence-generated vorticity corresponds to Prandtl's circulation of the second kind (Prandtl 1942, pp. 130–134).

(vi) The terms in the fifth line of equation (4), as well as the $\partial/\partial s$-terms in the first line relate to the downstream non-uniformity of the flow. They vanish for axisymmetric curved flow (defined by $\partial/\partial s = 0$), whence they are not essential to the mechanisms underlying the two cross-stream circulation cells.

(vii) The last line represents the dissipation by the molecular viscosity.

The literature on cross-stream circulation either directly refers to this vorticity equation, or the findings reported put in terms of it. Therefore, it makes sense to summarize the current state of knowledge before continuing on the energy transfer between mean flow and turbulence.

## 3. Current state of knowledge

Three-dimensional numerical models, especially for closed-conduit flow, are capable of reproducing secondary flow. The results, however, depend critically on the model formulation, especially the turbulence closure and the treatment of the boundary conditions. Therefore, it is worthwhile to analyse the mechanisms that lead to these secondary flow phenomena. Since these mechanisms are different for the centre-region cell and the outer-bank cell, these two cells will be treated separately in the following description of the state of the art.

### 3.1. *Centre-region cell*

The centre-region cell has been thoroughly investigated in the past, with Boussinesq (1868) and Thomson (1876) as pioneers. Its formation is usually explained by the local imbalance between the centrifugal force and the cross-stream pressure gradient, represented by the simplified transverse momentum equation (cf. equation (1))

$$0 = \frac{1}{1+n/R}\frac{v_s^2}{R} - \frac{1}{\rho}\frac{\partial p}{\partial n} - \frac{\partial \overline{v_n' v_z'}}{\partial z} + \nu\nabla^2 v_n. \tag{7}$$

The corresponding simplified downstream vorticity equation (cf. equations (4)–(6)) is

$$0 = -\frac{1}{1+n/R}\frac{\partial}{\partial z}\left(\frac{v_s^2}{R}\right) + \frac{\partial^2 \overline{v_n' v_z'}}{\partial z^2} + \nu\nabla^2 \omega_s. \tag{8}$$

This equation expresses the balance between vorticity generation by the centrifugal force and vorticity dissipation by the turbulent shear stress and the molecular viscosity, respectively. The mechanism is similar in laminar and turbulent curved flow. Assuming a hydrostatic pressure distribution, a vertical profile of the downstream velocity and, in the case of turbulent flow, the eddy viscosity, the vertical profile of the cross-stream velocity in the central part of the centre-region cell can be solved from either of the above equations.

Models that treat the cross-stream velocity as a first-order perturbation to the downstream velocity profile for straight flow are called linear. Such models, which ignore higher-order feedback, have been proposed by among others, Rozovskii (1957), Engelund (1974), Kikkawa, Ikeda & Kitagawa (1976), de Vriend (1977), Falcon Ascanio & Kennedy (1983) and Johannesson & Parker (1989). Kalkwijk & de Vriend (1980) and Ikeda, Yamasaka & Kennedy (1990) propose basically similar models that are claimed to be valid throughout the cross-section. These linear models only give good results for very mildly curved bends, but overestimate the strength of the centre-region cell for moderately to strongly curved bends, as illustrated by the experimental data of de Vriend (1981a), Booij & Tukker (1996), Blanckaert (2001) and Blanckaert & de Vriend (2004).

Their overestimation is a consequence of neglecting the nonlinear feedback between the downstream velocity and the centre-region cell (cf. de Vriend 1981*a*). Advective momentum transport by the centre-region cell deforms the $v_s$-profile, decreasing the velocity in the upper part of the water column and increasing it in the lower part (Blanckaert & Graf 2004; cf. figure 3*c* in §6). This deformation of the $v_s$-profile reduces the vertical gradient of the centrifugal force, $(\partial/\partial z)(v_s^2 / |R|)$, which, according to equation (8), is the driving mechanism for the cross-stream circulation.

Blanckaert & de Vriend (2004) propose a nonlinear model that accounts for this feedback. Similar to the linear models, a vertical profile of the eddy viscosity is assumed. However, instead of prescribing a straight-flow $v_s$-profile, they calculate the deformed $v_s$-profile from a simplified downstream momentum equation that accounts for advective momentum redistribution by the centre-region cell. This deformed $v_s$-profile is subsequently inserted into equation (8), yielding the vertical profile of the cross-stream velocity in the central part of the centre-region cell. This model compares rather well with experimental data for moderately to strongly curved flow (Blanckaert & Graf 2004; Blanckaert & de Vriend 2004).

Although this comparison with data is promising, it is not clear to what extent the nonlinear model captures all mechanisms relevant to the formation of the centre-region cell. Especially, the effects of neglecting advective transport in equations (7) and (8) and the rather basic modelling of turbulence need further investigation.

### 3.2. *Outer-bank cell*

Outer-bank cells have often been observed in curved turbulent flow and are believed to play an important role in the stability of the outer bank (Bathurst, Thorne & Hey 1979; de Vriend 1981*a, b*; Christensen *et al.* 1999; Blanckaert & Graf 2004). Yet, little is known about the underlying mechanisms and the conditions under which these cells occur. This can be attributed to the difficulty of accurately measuring the velocities and the turbulent stresses involved (further, see Blanckaert & Graf 2001). Both skewing-induced and turbulence-induced vorticity generation must be expected to play a role. Similar cells have been observed in curved laminar flow and in straight turbulent flow, which can be seen as asymptotic cases showing either one of the vorticity-generating mechanisms. Before considering curved turbulent flow, we will briefly summarize the literature on both of these asymptotic cases.

#### 3.2.1. *Curved laminar flow*

The control parameter of outer-bank cell formation in curved laminar flow is the Dean number, defined as the product of the Reynolds number and the square root of a curvature ratio, e.g. $De = Re(H/R)^{0.5}$, or $De = Re(B/R)^{0.5}$. Physically, it can be interpreted as the ratio between the centrifugal effect, which favours the outer-cell formation, and the molecular dissipation, which opposes it. Numerical investigations have been made by Cheng, Lin & Ou (1976), de Vriend (1981*b*) and Winters (1987) for the case of axisymmetric curved flow ($\partial/\partial s = 0$). They show that, on increasing the Dean number, the outer-bank cell suddenly comes into existence at a critical value of *De*. As the curvature increases, advective redistribution of momentum by the secondary flow deforms the $v_s$-profiles, and correspondingly decreases the driving centrifugal term $(\partial/\partial z)(v_s^2/|R|)$ in the vorticity equation. The outer-bank cell comes into existence when the $v_s$-profiles are so strongly deformed that the driving term changes sign in the upper part of the water column (cf. figure 3*c* in §6). For the axisymmetric curved flows investigated in these numerical models, the outer-bank cell was only slightly weaker than the centre-region cell. These numerical results have

been confirmed by an experimental investigation of the flow in a $180°$ curved duct by Hille, Vehrenkamp & Schulz-Dubois (1985). However, they found the outer-bank cell to be much weaker than the centre-region cell in most of the bend, and only gain strength beyond $120°$.

### 3.2.2. *Straight turbulent flow*

Prandtl (1942) suggests that the near-bank circulation cells in straight turbulent flow are caused by turbulence. Einstein & Li (1958) show in a rigorous analysis that gradients of turbulent stresses generate the corresponding downstream vorticity. Ever since, the role of the cross-stream turbulence terms in the downstream vorticity equation has been investigated extensively, in experiments as well as in numerical models.

Due to the difficulty in accurately measuring the turbulent stresses, most experiments have been carried out in uniform airflow (closed conduits) and seldom include measurements of $\overline{v'_n v'_z}$ (except Perkins 1970). Demuren & Rodi (1984) summarize the experimental findings of Brundett & Baines (1964), Gessner & Jones (1965), Perkins (1970) and Gessner (1973), stating that the dominant terms in the downstream vorticity equation (4) include $\overline{v'^2_n} - \overline{v'^2_z}$ and $\overline{v'_n v'_z}$, which are almost equal and of opposite sign. The difference is of the same order of magnitude as the advective terms $v_n \partial \omega_s / \partial n + v_z \partial \omega_s / \partial z$ and drives the near-bank cells. Nezu & Nakagawa (1984) and Nezu, Nakagawa & Tominaga (1985) analyse the downstream vorticity equation in airflow experiments in rectangular ducts, whereas Tominaga *et al.* (1989) use open-channel flow experiments with different boundary roughnesses, aspect ratios and sidewall inclinations. They could not measure the turbulent shear stress $\overline{v'_n v'_z}$ and suggest that $\overline{v'^2_n} - \overline{v'^2_z}$ is the source of the cross-stream circulation and that $\overline{v'_n v'_z}$ acts as a dissipator (also see Nezu & Nakagawa 1993). Bradshaw (1987), on the other hand, points out that the relative contributions of $\overline{v'^2_n} - \overline{v'^2_z}$ and $\overline{v'_n v'_z}$ only depends on the orientation of the $n$- and $z$-axes, as is readily illustrated by representing the cross-stream turbulent stress components on a Mohr circle.

Nezu & Nakagawa (1993) highlight the importance of the free water surface, by comparing the turbulence-generated cross-stream circulation cells in open channels with those in curved ducts. Furthermore, they give a detailed description of the interactions between the cross-stream circulation, the cross-stream turbulence, the distributions of the mean flow and the boundary shear stress, the boundary properties, the channel geometry, etc.

Naot & Rodi (1982) and Demuren & Rodi (1984) claim that the turbulence-generated near-bank cells in straight turbulent flow cannot be simulated with linear eddy viscosity models, i.e. models assuming a linear stress–strain relationship. They succeed in simulating them with an Algebraic Stress Model. Speziale (1987) attributes this failure of linear eddy viscosity models (such as the linear $k-\varepsilon$ model) to their inability to correctly represent the turbulent normal stresses and proposes nonlinear turbulence models ($k-\varepsilon$ and $k-l$ models) that are able to simulate the near-bank cells. Indeed, Colombini (1993) succeeds in simulating these cells with such a nonlinear turbulence model. Kawahara & Tamai (1988) demonstrate mathematically that linear eddy viscosity models cannot simulate turbulence-induced cross-stream circulation.

These theoretical, experimental and numerical investigations lead to the following hypothesis concerning the formation of near-bank circulation cells in straight uniform turbulent flow. Since the advective transport only redistributes vorticity over the cross-section and is fundamentally unable to generate or dissipate vorticity, the cross-stream turbulent stresses, $\overline{v'^2_n} - \overline{v'^2_z}$ and $\overline{v'_n v'_z}$, have to account for both the generation and the

dissipation of vorticity. The vorticity equation, however, does not indicate whether the cross-stream turbulence terms generate or dissipate mean downstream vorticity $\omega_s$. Physically speaking, no distinction can be made between the role of the turbulent normal stresses $\overline{v_n'^2} - \overline{v_z'^2}$ and the role of the turbulent shear stress $\overline{v_n' v_z'}$, since their relative magnitudes uniquely depend on the orientation of the $n$- and $z$-axes. Locally, the difference between the terms including $\overline{v_n'^2} - \overline{v_z'^2}$ and $\overline{v_n' v_z'}$ is balanced by the advective transport terms.

### 3.2.3. *Curved turbulent flow*

The bi-cellular pattern of cross-stream circulation has often been observed in curved turbulent flow, in laboratory experiments (Mockmore 1943; Einstein & Harder 1954; Rozovskii 1957; Götz 1975; Choudhary & Narasimhan 1977; Siebert 1982; Booij & Tukker 1996; Shiono & Muto 1998; Tominaga, Nagao & Nezu 1999; Booij 2003), as well as in the field (Bathurst *et al.* 1979; Dietrich & Smith 1983; de Vriend & Geldof 1983). Yet, little is known about the mechanisms underlying it, nor about the conditions for its occurrence.

Götz (1975) suggests that the occurrence depends on the aspect ratio, whereas Bathurst *et al.* (1979) suggest that the outer-bank cell only occurs near steep banks, not near shelving banks. In an attempt to define a quantitative criterion of occurrence, de Vriend (1981*a*) assumes the mechanisms to be the same as in curved laminar flow, where the outer-bank cell is generated by the centrifugal force only. Assuming the cross-stream turbulent stresses to act in a similar (purely dissipative) way as the molecular stresses in laminar flow, he replaces the molecular viscosity in the Dean number by the depth-averaged turbulent eddy viscosity in straight uniform flow. From observations of the outer-bank cell in mildly curved bends, however, combined with his failure to simulate the observed pattern with fully three-dimensional numerical models with a linear turbulence closure, de Vriend concludes that the outer-bank cell cannot be explained from the centrifugal force only. Because the observed outer-bank cells in bends are stronger than in the corresponding straight-channel flow, they cannot be exclusively turbulence-generated, either.

This led to the hypothesis that the outer-bank cell in curved turbulent flow is generated by the combined action of the centrifugal force (vortex-skewing) and turbulence. Christensen *et al.* (1999) carried out numerical simulations of the outer-bank cell with a linear $k-\varepsilon$ closure and with a Reynolds Stress Model. From the differences between the results they conclude that the outer-bank cell is not uniquely skewing-induced, but that turbulent vorticity-generation plays an important role. Jia, Blanckaert & Wang (2001) successfully simulated the outer-bank cell observed in the present experiment with a nonlinear $k-\varepsilon$ closure.

From this literature review, it can be concluded that the isolated behaviour of the centrifugal term and the cross-stream turbulence terms is relatively well understood. The insight into the physics of curved-flow turbulence and its interaction with the centrifugal force, however, needs further development.

## 4. Kinetic energy transfer between mean flow and turbulence

The above considerations on the downstream vorticity equation have shown that downstream vorticity in curved flow is generated by the centrifugal force (skewing), and redistributed over the cross-section by the advective transport terms. To maintain the vorticity balance, there must be dissipation by the turbulent stresses. In the case of the near-bank cells in straight uniform flow, however, turbulent stresses are also

responsible for the generation of vorticity. It is not clear *a priori* from the vorticity equation whether locally the turbulent stresses in total increase or decrease the mean vorticity.

By definition, the mean cross-stream motion $(v_n, v_z)$ contains mean-flow kinetic energy, $(v_n^2 + v_z^2)/2$, whereas the cross-stream turbulent stresses correspond to the cross-stream velocity fluctuations $(v_n', v_z')$ and thus contain turbulent kinetic energy, $(\overline{v_n'^2} + \overline{v_z'^2})/2$. Hence, turbulence-induced near-bank circulation cells like those in straight uniform flow require a transfer of kinetic energy from turbulence to the mean flow.

Although previous investigations on cross-stream circulation cells were limited to the vorticity equation, further insight may be gained by looking into the transfer of kinetic energy between turbulence and the mean flow. Terms representing this transfer appear with opposite signs in the dynamic equations for the mean flow and the turbulent kinetic energy. In the turbulent kinetic energy equation, they appear as (Hinze 1975, chap. 1–13)

$$\mathscr{P} = -\left\lfloor \left(\overline{v_s'^2} - \tfrac{2}{3}k\right)e_{ss} + \left(\overline{v_n'^2} - \tfrac{2}{3}k\right)e_{nn} + \left(\overline{v_z'^2} - \tfrac{2}{3}k\right)e_{zz} \right. \\ \left. + 2\overline{v_s'v_n'}\,e_{sn} + 2\overline{v_s'v_z'}\,e_{sz} + 2\overline{v_n'v_z'}\,e_{nz}\right\rfloor, \quad (9)$$

in which the turbulent kinetic energy, $k$, and the strain rates, $e_{jk}$ ($j, k = s, n, z$), are defined as (Batchelor 1970, p. 600)

$$k = \tfrac{1}{2}\left(\overline{v_s'^2} + \overline{v_n'^2} + \overline{v_z'^2}\right), \quad (10)$$

$$\left.\begin{aligned}
e_{ss} &= \frac{1}{1+n/R}\frac{\partial v_s}{\partial s} + \frac{1}{1+n/R}\frac{v_n}{R}, \qquad e_{nn} = \frac{\partial v_n}{\partial n}, \\
e_{sn} &= \frac{1}{2}\left(\frac{1}{1+n/R}\frac{\partial v_n}{\partial s} + \frac{\partial v_s}{\partial n} - \frac{1}{1+n/R}\frac{v_s}{R}\right) \\
e_{sz} &= \frac{1}{2}\left(\frac{1}{1+n/R}\frac{\partial v_z}{\partial s} + \frac{\partial v_s}{\partial z}\right), \qquad e_{nz} = \frac{1}{2}\left(\frac{\partial v_z}{\partial n} + \frac{\partial v_n}{\partial z}\right), \qquad e_{zz} = \frac{\partial v_z}{\partial z}.
\end{aligned}\right\} \quad (11)$$

Equation (9) indicates that the energy fluxes per unit mass take place through work done by the turbulent stresses as the mean flow deforms. The sum of these energy fluxes is (mostly) positive, i.e. from mean flow to turbulence, and is commonly called the production or generation of turbulent kinetic energy. The sign of the kinetic energy transfer via the cross-stream turbulent stresses, $\overline{v_n'^2}$, $\overline{v_z'^2}$ and $\overline{v_n'v_z'}$, is expected to be especially important with respect to the turbulence-induced vorticity.

A comparison of the energy transfer related to the cross-stream turbulence with that primarily related to boundary friction (the $\overline{v_s'v_z'}$- and $\overline{v_s'v_n'}$-terms) must give indications of the importance with respect to the total energy loss in a bend. This will be discussed later on in the paper.

The kinetic energy fluxes between mean flow and turbulence have important implications for the numerical modelling of turbulence. Turbulence closure models often make use of mixing coefficients, defined as the ratio between the deviatoric turbulent stresses and the corresponding strain rates:

$$\nu_{jk} = \nu_{kj} = -\frac{\overline{v_j'v_k'} - 2/3\delta_{jk}k}{2e_{jk}} \quad (j, k = s, n, z) \quad (12)$$

where $\delta_{jk}$ is the Kronecker delta. With this definition, the production of turbulent kinetic energy (9), can be rewritten as

$$\mathscr{P} = 2\left(v_{ss}e_{ss}^2 + v_{nn}e_{nn}^2 + v_{zz}e_{zz}^2 + 2v_{sn}e_{sn}^2 + 2v_{sz}e_{sz}^2 + 2v_{nz}e_{nz}^2\right). \tag{13}$$

The sign of the mixing coefficient $v_{jk}$ indicates the sense of the corresponding kinetic energy flux. Applying a scalar eddy viscosity for turbulence closure implies that $v_{ss} = v_{nn} = v_{zz} = v_{sn} = v_{sz} = v_{nz} = v_t > 0$ and that all kinetic energy fluxes are definitely positive:

$$\mathscr{P} = 2v_t\left(e_{ss}^2 + e_{nn}^2 + e_{zz}^2 + 2e_{sn}^2 + 2e_{sz}^2 + 2e_{nz}^2\right) > 0. \tag{14}$$

This implies that, when using a linear eddy viscosity concept, kinetic energy is always transferred from the mean flow to the turbulence. By implication, the cross-stream turbulence terms in the downstream vorticity equation (4) are always dissipative. This means that this concept is not applicable to flows in which turbulence somehow contributes to the mean kinetic energy.

## 5. Combined analysis

From the above review of the current state of knowledge it can be concluded that the mechanisms underlying the centre-region cell and the outer-bank cell are not yet fully understood. Research so far has mostly been restricted to the downstream vorticity equation, whereas a simultaneous analysis of the downstream vorticity dynamics (cf. equations (4)–(6)) and the kinetic energy transfer between mean flow and turbulence (cf. equation (9)) seems to make more sense. Therefore, we will pursue this combined analysis in the remainder of the paper, based on the data from the experiment described hereafter.

The following issues will be addressed:

(i) What are the relevant mechanisms behind the generation of the centre-region cell? Does the simplified vorticity equation (8) capture all relevant mechanisms? What are the roles of advective transport and turbulence?

(ii) Can the hypothesis of de Vriend (1981a) and Christensen *et al.* (1999) that the outer-bank cell formation is associated with both skewing-induced and turbulence-induced vorticity be confirmed or rejected? What is the interaction between the two mechanisms?

(iii) What is the role of the cross-stream turbulence terms, $\overline{v_n'^2} - \overline{v_z'^2}$ and $\overline{v_n'v_z'}$, in the generation of turbulence-induced vorticity? The availability of data on all turbulent stress components must enable investigating this role in further depth.

(iv) To what extent does the cross-stream turbulence dissipate or generate vorticity? A combined analysis of the downstream vorticity dynamics and the transfer of kinetic energy between mean flow and turbulence must give further insight.

(v) How can strongly curved open-channel flow, and especially the outer-bank cell, be modelled numerically?

## 6. Experimental data

### 6.1. *The experiment*

The experimental set-up, the instrumentation, the measuring grids, the data treatment procedures and the distributions of the mean velocity components and the turbulent stress components have been treated in a separate paper (Blanckaert & Graf 2001). Therefore, only aspects that are of particular relevance to the present analysis will be repeated here.
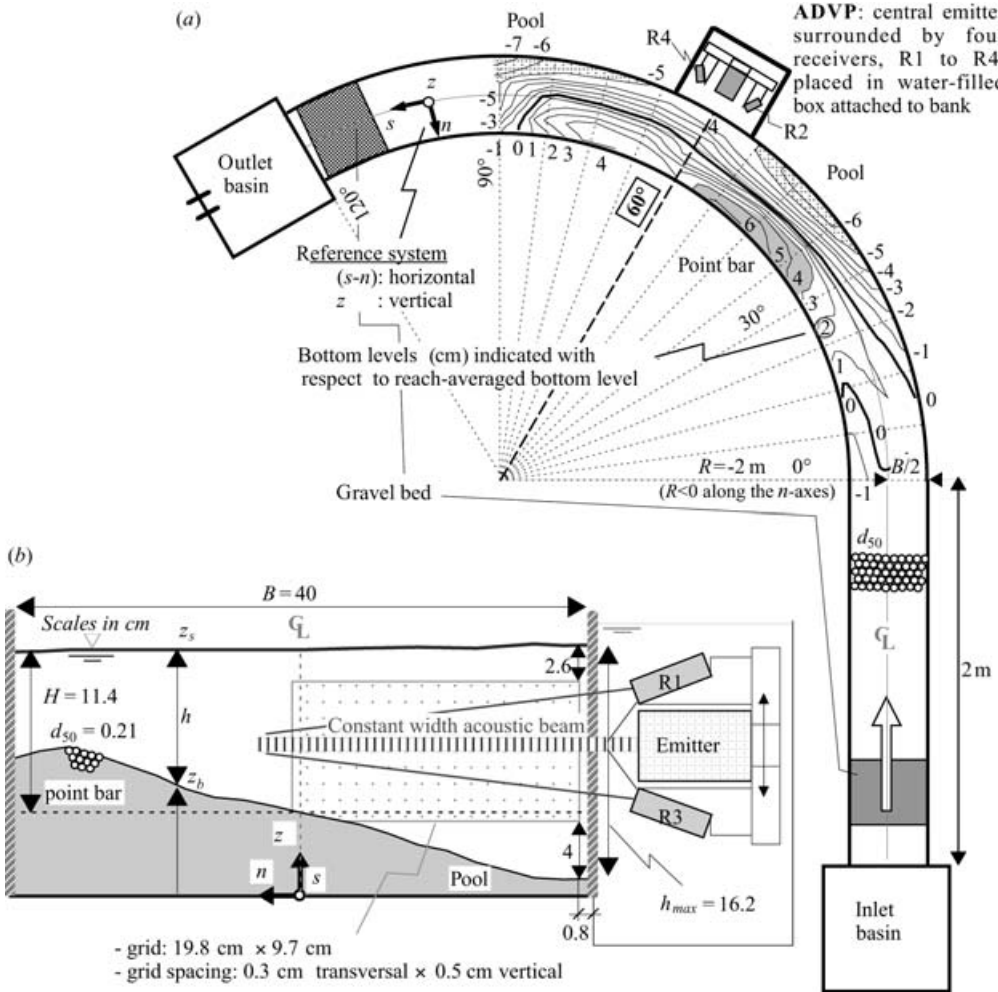
FIGURE 2. (*a*) Experimental set-up, bottom topography and reference system. (*b*) Measuring section at 60° and acoustic Doppler velocity profiler (ADVP) set-up.

Flow measurements were performed in a laboratory flume 0.4 m wide, consisting of a 2 m long straight approach reach, followed by a 120° bend to the left of constant curvature (radius 2 m). In a preliminary run, the initially horizontal sand bottom was deformed by the flow, via a process of so-called clear-water scour. Ultimately, the sediment transport vanished throughout and a stable (zero-time-derivative) bottom topography that significantly varies in the downstream direction was obtained (figure 2).

At first sight, it may seem more appealing to investigate axisymmetric curved flow, which does not continue to vary in the downstream direction ($\partial/\partial s$ terms vanish in equations (4) and (6)). However, the flow pattern in axisymmetric flow is not relevant to that in natural bends since the centre-region cell is significantly weaker and the outer-bank cell significantly stronger (Blanckaert 2002*b*; Christensen *et al.* 1999). We have deliberately opted to investigate a 'natural' flow, even though we are not able to estimate the downstream derivatives in the vorticity equations (4) and (6). Since these

| $R$ [m] | $B$ [m] | $d_{50}$ [mm] | $Q$ [l s$^{-1}$] | $H$ [m] | $S_s$ [‰] | $U$ [m s$^{-1}$] | $C_f$ | $Re$ [×10$^3$] | $Re_*$ | $Fr$ | $R/B$ | $R/H$ | $B/H$ |
|---|---|---|---|---|---|---|---|---|---|---|---|---|---|
| −2.0 | 0.40 | 2.1 | 17 | 0.11 | 1.89 | 0.38 | 0.008 | 42 | 70 | 0.36 | 5 | 17.9 | 3.6 |

$R$: centreline radius of curvature (negative along the $n$-axis)
$B$: channel width
$d_{50}$: median grain size diameter of the bed material
$Q$: flow discharge
$H$: overall mean flow depth ≈ depth at centreline
$S_s$: overall mean water-surface slope at the centreline
$U$: overall mean velocity

$C_f$: friction factor (estimated by Blanckaert & Graf 2001)
$\tau_b$: bottom shear stress, $\tau_b/\rho = u_*^2 = C_f U^2$
$Fr = U / (gH)^{1/2}$: overall mean Froude number
$Re = UH / \nu$: overall mean flow Reynolds number
$Re_* = u_* k_s / \nu$: overall mean particle Reynolds number
$\nu$: molecular viscosity
$k_s$: Nikuradse equivalent sand roughness

TABLE 1. Hydraulic conditions.

downstream derivatives vanish for axisymmetric flow, however, they are not essential for the mechanisms underlying the two cross-stream circulation cells.

Table 1 shows the hydraulic conditions. Clearly, this involves a rather sharp bend, as is indicated by the parameter values $R/B = 5$ and $R/H = 17.9$ ($B$ is the channel width, $H$ is the reach-averaged water depth, which is equal to the depth at the channel axis in the investigated cross-section at 60°). With an aspect ratio $B/H = 3.6$, the flume is much narrower than typical natural open-channel bends. Yet, these ratios do occur in mountain rivers and man-made channels. Moreover, in a wide bend with a natural bottom topography, the shallow point bar is usually wide and most of the time the flow is concentrated in the deepest part of the cross-section, where a significant transversal bottom slope exists (figure 20 in Odgaard 1984; figure 8.2 in Dietrich 1987). The flow in the deepest part of the cross-section in the experiment is therefore considered to be representative of the flow in the deeper part of wider natural bends.

The key measuring device is an Acoustic Doppler Velocity Profiler (ADVP) that was specially designed for laboratory applications (Hurther & Lemmin 1998). The ADVP simultaneously measures profiles along its main axis of the three quasi-instantaneous velocity components $v_j(t)$, from which the mean-velocity components $v_j$ and the turbulent stress components $\overline{v'_j v'_k}$ ($j, k = s, n, z$) can be derived. Detailed information on its working principle, its experimental uncertainty and a comparison with other velocity meters (see also the Appendix) can be found in Lemmin & Rolland (1997), Hurther & Lemmin (1998, 2001), Blanckaert & Graf (2001) and Blanckaert & Lemmin (2004). With this instrument non-intrusive velocity measurements were made in the outer half of the cross-section located at 60° from the bend entrance. The ADVP was mounted in a water-filled box attached to the outer bank. By traversing the ADVP vertically, radial profiles covering about half the channel width were taken every $\Delta z = 0.5$ cm. The measuring section, the measuring grid and the ADVP-configuration are shown in figure 2.

The present analysis requires the evaluation of the various terms in the vorticity equation, as well as the kinetic energy fluxes between mean flow and turbulence. These equations include derivatives of the measured quantities, which are difficult to evaluate directly from the raw data, because of the experimental scatter. The high spatial resolution of our data allowed an efficient smoothing by means of

two-dimensional splines with weight functions (de Boor 1978, Chaps 14 and 17). Derivatives of the measured quantities were obtained analytically from the description of the spline. Thanks to the weight functions, the measured data can be extended outside the measuring grid by imposing physical boundary conditions (such as the no-slip condition at rigid boundaries, no shear parallel to the water surface, etc.). Wherever this has been done, it is indicated in the relevant figures. For further information on the smoothing technique (including an example) and the extrapolations outside the measuring grid, we refer to Blanckaert & Graf (2001).

The uncertainty in the evaluated terms in equations (4)–(6) for the vorticity balance and equation (9) for the kinetic energy transfer is estimated in the Appendix as always better than 40%. This is sufficient for the purpose of this paper, since our interpretations focus on first-order effects.

## 6.2. *Experimental results*

The vectorial representation of the measured cross-stream velocity field, $(v_n, v_z)$, normalized by the overall mean velocity $U = Q/(BH)$, is shown in figure 3($d$). The centre-region cell reflects the 'classical' helical motion that is characteristic of flow in bends. The magnitude of the velocities involved is typically 10% of $U$. A region with weaker cross-stream velocities is found close to the outer bank. In the upper part of this outer-bank region an additional circulation cell can be observed, with a sense of rotation opposite to that of the centre-region cell. The velocities in this region are typically a few $\mathrm{cm\,s^{-1}}$.

The circulatory part of the cross-stream motion is reflected by the downstream vorticity, $\omega_s$, which is shown in figure 3($e$). The centre-region cell and the outer-bank cell, separated by the ($\omega_s = 0$)-contour, are clearly visible in the vorticity field. The vorticity increases towards the 'eye' of each cell and reaches maximum magnitudes of about $0.9\,U/H$ near the eye of the centre-region cell and $-0.22\,U/H$ near the eye of the outer-bank cell. Close to the outer-bank, $\omega_s$ assumes positive values, which represent the boundary layer near the bank, rather than an identifiable vortex.

The distribution of the normalized downstream velocity component, $v_s/U$, is given in figure 3($a$). Its depth-averaged value is nearly constant over most of the measuring area: $U_s/U \approx 1.35$ (figure 3$b$), which means that the depth-averaged velocity there is well above the overall mean velocity.

Figure 3($b$) also shows that the distribution of the normalized unit discharge, $U_s Bh/Q$, with $h$ denoting the local water depth, is concentrated in the deep outer part of the cross-section. Integration of this profile shows that about 80% of the discharge passes through the investigated outer half of the cross-section. The core of maximum velocity, marked by ✖ in figure 3($a, b$), is found near the transition between the two circulation cells. Figure 3($c$) compares some measured $v_s / U_s$-profiles with a logarithmic profile for a friction factor $C_f = 0.008$, which corresponds to the value in the experiment as estimated by Blanckaert & Graf (2001). The profiles shown are averaged over the outer-bank region ($n = -20$ to $-14$ cm), the transition zone ($n = -14$ to $-8$ cm) and the centre region ($n = -8$ to $0$ cm). The profiles in these three regions are rather similar: the measured velocities are well below the logarithmic profile in the upper part of the water column and well above it in the lower part. This deformation of the $v_s / U_s$-profiles is substantial, to the extent that the velocity maximum is found in the lower part of the water column. By analysing the downstream momentum equation on the basis of the measured data, Blanckaert & Graf (2004) show that this redistribution of the downstream velocity is mainly due to advective momentum transport by the two cross-stream circulation cells.
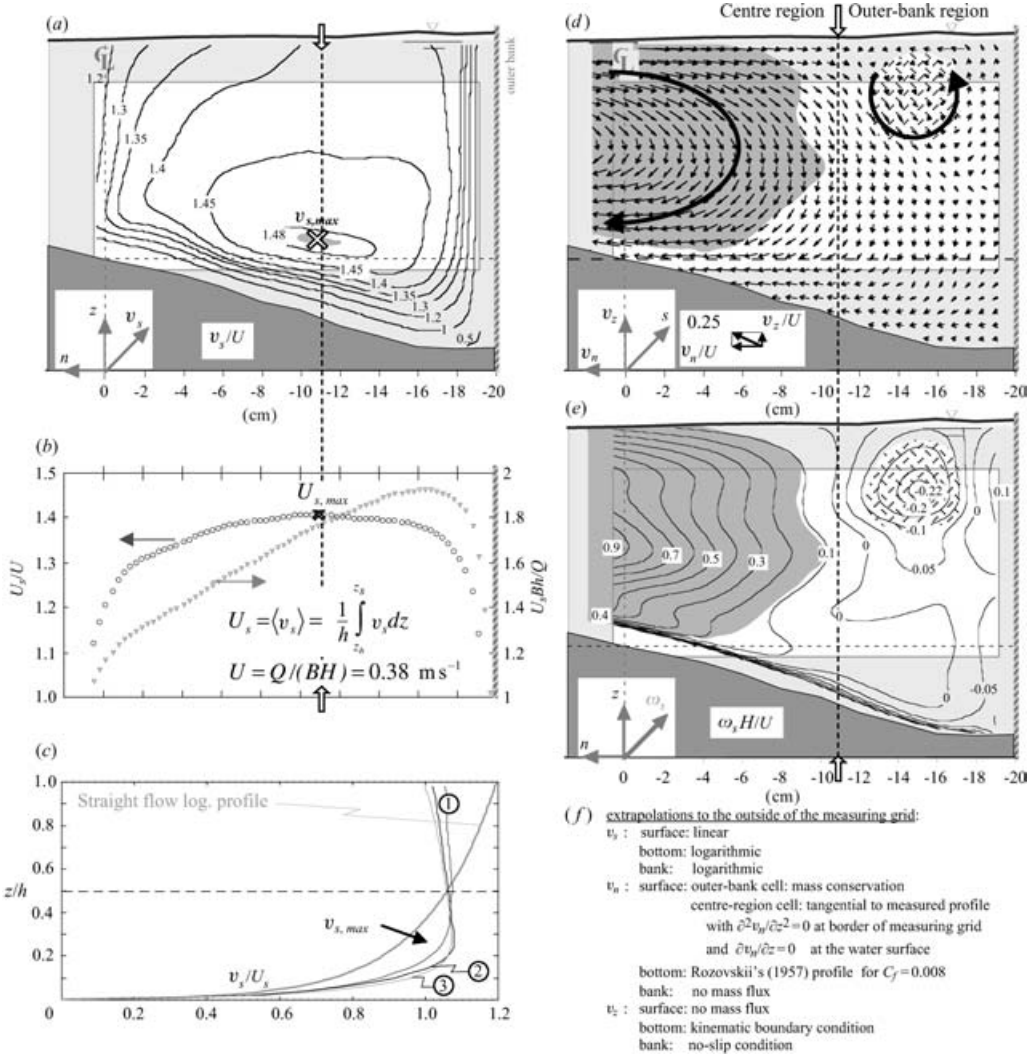
FIGURE 3. (*a*) Isolines of normalized downstream velocity, $v_s/U$. (*b*) Normalized depth-averaged downstream velocity, $U_s/U$; normalized unit discharge, $(U_s Bh)/Q$. (*c*) Vertical profiles of measured downstream velocity, $v_s/U_s$: 1 – outer-bank region ($-20$ to $-14$ cm); 2 – separation both regions ($-14$ to $-8$ cm); 3 – centre region ($-8$ to $0$ cm). (*d*) Vector representation of normalized cross-sectional motion, $(v_n, v_z)/U$. (*e*) Isolines of normalized downstream vorticity, $\omega_s H/U$. (*f*) Extrapolation outside measuring grid.

Figure 4(*a, b*) shows the distributions of the turbulence properties $\overline{v_n'^2} - \overline{v_z'^2}$ and $\overline{v_n' v_z'}$, which play an important role in the vorticity equation. They have been normalized by the characteristic shear velocity in the measuring section, $u_{*,60}$, which is defined as $u_{*,60} = \sqrt{g R_h (-\partial z_{S,60}/\partial s)}$, in which $-\partial z_{S,60}/\partial s$ is the downstream water-surface gradient at the centreline and $R_h$ is the hydraulic radius. In the experiment, this shear velocity was $0.045\ \mathrm{m\,s^{-1}}$. Near the flow boundaries, the velocity fluctuations perpendicular to the boundary are hindered by geometrical constraints. Near the bottom and near the water surface, this concerns the vertical fluctuations, so there $\overline{v_n'^2} > \overline{v_z'^2}$. In the region near the outer bank, the transverse fluctuations are hindered and $\overline{v_n'^2} < \overline{v_z'^2}$. The damping of the fluctuations by the water surface is only slightly weaker
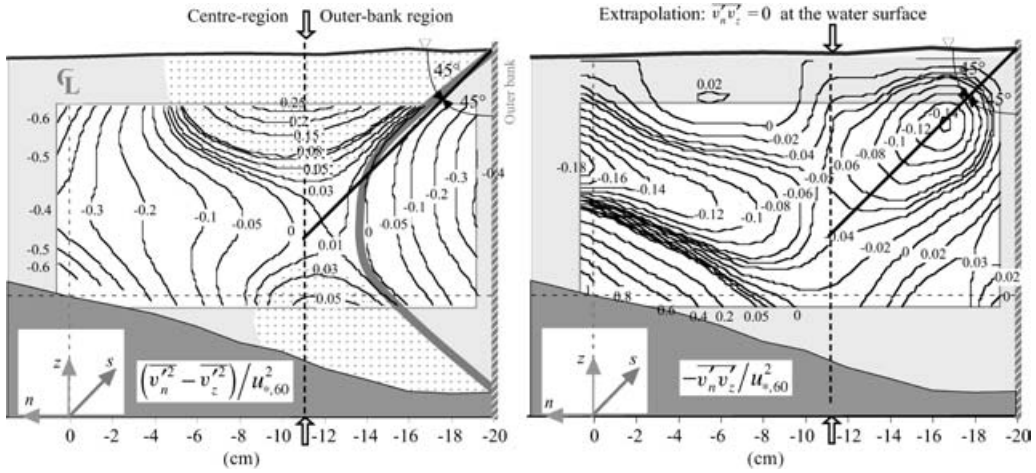
FIGURE 4. Isolines of normalized (*a*) turbulent normal stress difference, $(\overline{v_n'^2} - \overline{v_z'^2})/u_{*,60}^2$ (the thick grey line identifies $\overline{v_n'^2} = \overline{v_z'^2}$); (*b*) turbulent shear stress, $-\overline{v_n'v_z'}/u_{*,60}^2$.
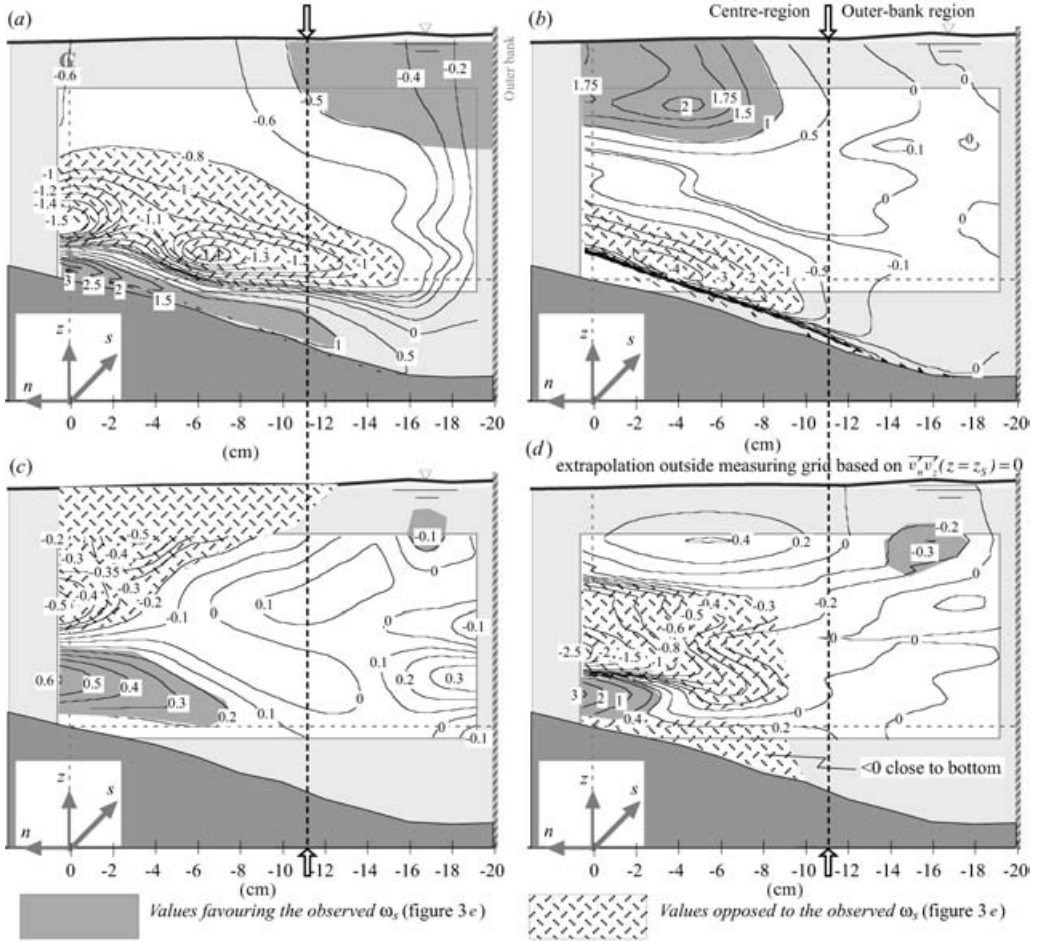
than that by the outer bank, and the line where $\overline{v_n'^2} = \overline{v_z'^2}$, drawn in figure 4(*a*), only slightly deviates from the bisector of the upper right corner of the flow domain. There, the pattern of $\overline{v_n'^2} - \overline{v_z'^2}$ is nearly antisymmetrical about this line. Similar patterns of $\overline{v_n'^2} - \overline{v_z'^2}$ have been observed in experiments with straight uniform flow (Nezu *et al.* 1985, for airflow in a duct; Tominaga *et al.* 1989, for open-channel flow). Nezu & Nakayama (1998, 1999) have shown that the damping by the water surface depends on the Froude number; at low Froude numbers, like in the present experiment, the water surface almost completely suppresses the nearby vertical fluctuations.

The turbulent shear stress $\overline{v_n'v_z'}$ seems to be correlated with the circulation cells. Even though the cells have a different sense of rotation, this turbulent shear stress does not change sign. Near the 'eye' of the weaker outer-bank cell, the absolute value is only slightly less than near the 'eye' of the centre-region cell. The pattern of $\overline{v_n'v_z'}$ is nearly symmetrical about the bisector of the upper right corner of the flow domain, which again indicates a similar influence of the water surface and the outer bank on the turbulent stresses. A similar near-corner pattern of $\overline{v_n'v_z'}$ has been measured by Nezu & Nakagawa (1984) in the case of airflow in a duct. It is to be expected that the influence of the water surface on $\overline{v_n'v_z'}$ also depends on the Froude number. In the region dominated by bottom friction, this stress component is primarily associated with the transverse component of the bottom shear stress. It is positive there, since the bottom shear stress is directed towards the centre of curvature, and so in the positive *n*-direction.

## 7. Analysis of the centre-region cell

### 7.1. *Observations (figures 3e, 5 and 6)*

Integrated over the water depth, the centrifugal term in the vorticity equations (4)–(6) is always positive, which complies with the sense of rotation of the centre-region cell. Due to advective momentum transport by the centre-region cell, the velocity maximum in the present experiments is in the lower part of the water column (figure 3*c*). As a

FIGURE 5. Isolines of normalized terms in downstream vorticity equations (4)–(6), multiplied by 10: (a) centrifugal term, (b) advective transport terms, (c) cross-stream turbulence anisotropy terms, (d) cross-stream turbulent shear stress terms.

consequence, the centrifugal term $-(\partial/\partial z)(v_s^2/R)$ in the vorticity equation is negative in a significant part of the water column (figure 5a), thus opposing the observed sense of rotation of the centre-region cell.

The advective transport terms in the vorticity equation, $v_n \partial \omega_s/\partial n + v_z \partial \omega_s / \partial z$, are of the same order of magnitude as the centrifugal term. The positive values in the upper part of the water column (figure 5b) compensate for the negative centrifugal term (figure 5a). This explains why the centre-region cell extends over the entire water depth, instead of splitting into two counter-rotating cells on top of each other. The
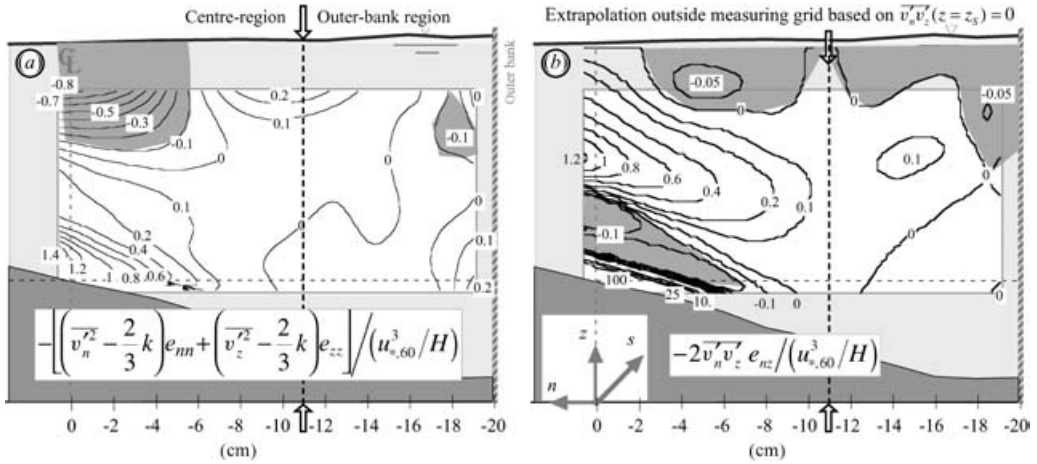
FIGURE 6. Isolines of the normalized kinetic energy fluxes between the mean flow and the turbulence via the cross-stream turbulent stresses (cf. equation (9)).

advective transport is generally dominated by the transverse contribution, $v_n \partial \omega_s / \partial n$. The vertical contribution, which is not shown separately in figure 5, is usually much smaller.

The role of the turbulent stress $\overline{v_n' v_z'}$ in the centre-region cell is complex. The $\overline{v_n' v_z'}$-terms are of leading order in the vorticity equation (figure 5$d$, cf. equation (8)). Close to the bottom, $\overline{v_n' v_z'}$ is associated with the transverse component of the bottom shear stress. Hence, the $\overline{v_n' v_z'}$-term in the vorticity equation opposes the observed vorticity in this layer, and mean-flow vorticity is dissipated into turbulence there (figure 6$b$). Just above that near-bottom layer, but still in the lower part of the water column, the $\overline{v_n' v_z'}$-term favours the observed vorticity. Analysis of the energy equation shows that a weak kinetic energy flux from turbulence to the mean flow occurs via $\overline{v_n' v_z'}$. In this zone, the centrifugal and $\overline{v_n' v_z'}$-terms agreeing with the sign of the existing vorticity are mainly balanced by the opposed advective transport term. As mentioned in the Appendix, the turbulence measurements in the lower 20% of the water column are less accurate and should therefore be interpreted with care. In most of the upper part of the water column, the $\overline{v_n' v_z'}$-term opposes the observed vorticity and mean-flow kinetic energy is transferred to turbulence.

The $(\overline{v_n'^2} - \overline{v_z'^2})$-terms in the vorticity equation are smaller than the other terms, but they are not negligible (cf. figure 5$c$). In the upper part of the water column, their sign is opposite to that of the observed (positive) vorticity. In the lower part of the water column, the sign of these terms complies with the observed vorticity.

### 7.2. *Modelling implications*

Based on equation (8), Blanckaert & de Vriend (2004) have proposed a nonlinear model for the centre-region cell that accounts for its feedback with the $v_s$-profile. By combining this model with a two-dimensional depth-averaged flow model, it should be possible to reproduce the velocity field in moderately curved flows with a reasonable accuracy. For curvatures that are so strong that the velocity maximum occurs in the lower part of the water column, like in the present experiment, it is essential to include the advective momentum transport terms in the transversal momentum equation. An accurate simulation of the centre-region cell, and of the flow field in general, now requires the use of the fully three-dimensional flow equations.

Turbulence is not purely dissipative. Restitution of kinetic energy from turbulence to the mean flow occurs in certain regions of the flow, accompanied by mean vorticity generation. The turbulence-generated vorticity, however, is relatively weak, so that a fully three-dimensional numerical model with a linear turbulence closure must be good enough to describe the centre-region cell, even in the case of strong curvature.

## 8. Analysis of the outer-bank cell

### 8.1. *Observations* (*figures 3e, 5 and* 6)

Except for the centrifugal term, all terms in the downstream vorticity equations (4)–(6) (also see figure 5) and all kinetic energy fluxes between mean flow and turbulence (cf. equation (9) and figure 6) are smaller in the outer-bank region than in the central region. The profiles of the downstream velocity in the outer-bank region are similar to those in the central region. The velocity maximum is located in the lower half of the water column and $\partial v_s / \partial z$ is slightly negative above that point. This implies that the sign of the centrifugal term in the vorticity equation complies with the sense of rotation of the outer-bank cell. In fact, this is the only mechanism that drives the outer-bank cell in laminar curved flow.

In the flow domain covered by the outer-bank cell, the advective transport of vorticity is negligible (figure 5b). Each of the cross-stream turbulence terms mainly assumes negative values of the same order of magnitude as the centrifugal term, which favour the outer-bank cell. As was shown before (cf. figure 4), the normal stress difference $v'^2_n - v'^2_z$ in the region occupied by the outer-bank cell is nearly antisymmetrical and the shear stress $\overline{v'_n v'_z}$ is nearly symmetrical about the bisector of the top right corner of the flow domain. If these distributions were perfectly antisymmetrical and symmetrical, respectively, like in a corner flow, antisymmetrical patterns of the corresponding terms in the vorticity equation would result in each case (as is easily demonstrated by interchanging the $n$- and $z$-indices). This indicates the sensitivity of turbulence-generated vorticity to the influence of the flow boundaries.

The kinetic energy transfer between mean flow and turbulence via the cross-stream turbulent stresses $v'^2_n$, $v'^2_z$ and $\overline{v'_n v'_z}$ is an order of magnitude smaller than in the centre region (figure 6). The occurrence of positive and negative contributions indicates that mean-flow energy in the outer-bank cell is produced as well as dissipated by the cross-stream turbulent stresses. The primary conclusion to be drawn, however, is that the exchange of energy between mean flow and turbulence is quite small in this area.

### 8.2. *Interpretation and modelling implications*

Our observations confirm the hypothesis of de Vriend (1981a) and Christensen *et al.* (1999) that both skew-induced and turbulence-induced vorticity contribute to the generation of the outer-bank cell. Moreover, both mechanisms strengthen each other through a positive feedback, as indicated by the following observation.

In steady flow, all terms on the right-hand-side of equations (4)–(6) should add up to zero. Even when taking the experimental uncertainty into account, the sum of the investigated terms is negative in the flow region occupied by the outer-bank cell. This non-zero sum is presumably mainly compensated by the non-uniformity term, $-(1 + n/R)^{-1} v_s \partial \omega_s / \partial s$, which was not measured. This indicates that the outer-bank cell further strengthens in the downstream direction, which is in line with the observed strengthening of the outer-bank cell along the bend in curved laminar flow (Hille *et al.* 1985) and with the observation that the outer-bank cell is much stronger in

axisymmetric flow ($\partial / \partial s = 0$). It also explains why the near-bank cell in turbulent curved flow is stronger than in the corresponding straight-channel flow.

For the present case of a channel with vertical sidewalls and a straight inflow reach followed by a constant-curvature bend, this positive feedback can be explained as follows. In the straight inflow reach, near-bank circulation cells are induced by the cross-stream turbulence. By advecting flow momentum, they deform the $v_s$-profiles, yielding a negative velocity gradient $\partial v_s/\partial z$ in the upper part of the water column. Upon entering the bend, this negative gradient gives rise to a centrifugal force that enhances the outer-bank cell, hence the deformation of the $v_s$-profile, etc. This positive feedback between the cell and the centrifugal force tends to intensify the outer-bank cell along the bend. Such an interaction between the two mechanisms has already been suggested by de Vriend (1981a) for weakly curved flow.

Our observations show that the cross-stream turbulent stresses $\overline{v_n'^2} - \overline{v_z'^2}$ and $\overline{v_n'v_z'}$ have a similar role in the vorticity balance. Hence, turbulence anisotropy is indeed the physical cause of turbulence-induced vorticity. Slight asymmetries may be relevant to the resulting vorticity pattern, which indicates the importance of accurately modelling the boundary conditions in numerical simulations. Also the kinetic energy fluxes via these turbulent stresses are similar and contribute to the generation as well as the dissipation of mean-flow vorticity. The primary observation, however, is that the energy fluxes between mean flow and turbulence over these cross-stream turbulent stresses are quite small in this area.

Speziale (1987) attributes the failure of linear turbulence models to represent turbulence-induced vorticity to their inability to link a non-zero turbulence anisotropy, $\overline{v_n'^2} - \overline{v_z'^2}$, to the downstream velocity field. Based on our combined analysis of the vorticity dynamics and the kinetic energy transfer between mean flow and turbulence, this hypothesis can be refined and complemented.

Although linear turbulence models are unable to correctly represent the turbulent normal stresses, there is no physical reason why they should yield a zero cross-stream turbulence anisotropy:

$$\overline{v_{n^*}'^2} - \overline{v_{z^*}'^2} = -2\nu_t \left( \frac{\partial v_{n^*}}{\partial n^*} - \frac{\partial v_{z^*}}{\partial z^*} \right) \neq 0. \tag{15}$$

Consider for example a point in the central part of the centre-region cell, where $v_z \approx 0$. Obviously, $\partial v_n/\partial z \neq 0$ and, when using a linear eddy viscosity model, $\overline{v_n'v_z'} = -\nu_t(\partial v_n / \partial z + \partial v_z/\partial n) \neq 0$. Via the Mohr-circle representation, it can easily be shown that this implies a non-zero turbulence anisotropy $\overline{v_{n^*}'^2} - \overline{v_{z^*}'^2} \neq 0$, with the $(n^*, z^*)$-coordinates along the principal axes of the turbulent stress tensor. As a consequence, these models' inability to correctly represent the turbulent normal stresses does not explain why they cannot predict turbulence-generated cross-stream circulation cells (be it incorrect ones).

Nonetheless, in the case of straight uniform flow considered by Speziale, linear turbulence models do not reproduce the near-bank circulation cells, i.e. $(v_n, v_z) = 0$ and consequently also $\overline{v_n'^2} - \overline{v_z'^2} = -2\nu_t(\partial v_n/\partial n - \partial v_z/\partial z) = 0$. This heuristic observation, however, does not prove that it is impossible for these models to simulate turbulence-generated circulation. Introducing a perturbation to the flow, $(\hat{v}_n, \hat{v}_z) \neq 0$, such that $\hat{\omega}_s \neq 0$ and $\widehat{v_n'^2} - \widehat{v_z'^2} = -2\nu_t(\partial \hat{v}_n / \partial n - \partial \hat{v}_z / \partial z) \neq 0$, will generally give rise to the generation and/or dissipation of mean-flow vorticity. The numerical model shows that the perturbation dampens out, whence the turbulent stresses must be dissipative.

The analysis of our experimental data indicates that, in the region of the outer-bank cell, the (weak) kinetic energy fluxes due to the cross-stream turbulent stresses are directed both from the mean flow to the turbulence and inversely. Hence, the cross-stream turbulent stresses contribute to the generation as well as the dissipation of the outer-bank cell. Kinetic energy fluxes from the turbulence to the mean flow have been observed in various other experiments in open-channel bends (Anwar 1986; Booij & Tukker 1996; Booij 2003; and Shiono & Muto 1998 for the case of overbank flow in a meander).

Our observations and the above analysis show that, in addition to Speziale's (1987) necessary condition, there is a second necessary condition for turbulence models to reproduce turbulence-generated vorticity: the turbulence model must be able to represent fluxes of kinetic energy from turbulence to the mean flow. This is confirmed by the results of Kawahara & Tamai (1988), who demonstrate theoretically that linear eddy viscosity models cannot represent turbulence-induced vorticity, unless negative mixing coefficients are allowed (cf. equation (14)).

Nonlinear turbulence models, based on a nonlinear relationship between the turbulent stresses and the strain rates, seem to satisfy both conditions. At least, they correctly predict the near-bank cells in turbulent straight flow (Speziale 1987; Colombini 1993), as well as the outer-bank cell in the present experiment (Jia *et al.* 2001). Higher-order turbulence models also seem to satisfy both conditions: Naot & Rodi (1982) and Demuren & Rodi (1984) simulated the near-bank cells in turbulent straight flow with an algebraic stress model, and Christensen *et al.* (1999) simulated outer-bank cells in turbulent curved flow with a Reynolds stress model, even for weak curvature. They have also succeeded in simulating the outer-bank cell in a bend with a standard linear $k-\varepsilon$ model, but only for very strong curvature ratios ($R/H < 16$). With the $k-\varepsilon$ model, a very strong skewing-induced vorticity generation is needed to overcome the vorticity dissipation by the cross-stream turbulence. This is in line with the above conclusions.

The following observation on the cross-stream circulation cells in straight uniform flow also points to the dominant role of the energy fluxes. Our measurements show that the effects of the water surface and the outer bank on the cross-stream turbulence, $\overline{v_n'^2} - \overline{v_z'^2}$ and $\overline{v_n'v_z'}$ (cf. figure 4), are nearly identical. The distributions of the corresponding cross-stream turbulence terms in the downstream vorticity equation will thus be nearly identical in a corner formed by two fixed boundaries and in one formed by a water surface and a fixed boundary. Yet, Tominaga *et al.* (1989) and Nezu & Nakagawa (1993) have shown that in straight uniform flow the resulting vorticity patterns are significantly different. Two identical counter-rotating circulation cells exist in a corner formed by two fixed boundaries, whereas in an open-channel corner the circulation cell near the free water surface is dominant over the counter-rotating one near the bank. These different vorticity patterns can be explained by slight asymmetries in the patterns of $\overline{v_n'^2} - \overline{v_z'^2}$ and $\overline{v_n'v_z'}$, but especially by differences in the kinetic energy fluxes. Near the water surface, the kinetic energy fluxes are smaller than near the fixed boundary, where the no-slip condition gives rise to much steeper mean velocity gradients.

In summary, we can conclude from the present analysis that the proximity of flow boundaries modifies the turbulence characteristics, which, in their turn, influence the downstream vorticity field, and thus the cross-stream motion ($v_n, v_z$). In the case of a bend with a vertical outer wall, this results in the formation of an outer-bank cell. The above findings indicate that the vorticity pattern cannot be explained by considering only the vorticity equation, as has been done in previous investigations: the kinetic

energy transfer plays an essential role. An accurate description of the effects of boundary proximity on the turbulence characteristics, and especially on the kinetic energy transfer, is therefore a prerequisite to the accurate modelling of the flow field in the vicinity of the outer bank.

## 9. Kinetic energy transfer

Our analysis shows that the accurate modelling of the kinetic energy fluxes between mean flow and turbulence is the key to the accurate simulation of the cross-stream circulation cells, especially the one near the outer bank. In order to estimate how the production of turbulent kinetic energy is composed, the contributions of the cross-stream turbulent stress components, $\overline{v_n'^2}$, $\overline{v_z'^2}$ and $\overline{v_n' v_z'}$ (cf. figure 6), will be compared with the main contributions related to friction at the flow boundaries.

In straight uniform flow through a vertical slice without lateral friction, turbulence is produced by bottom friction and represented by the kinetic energy flux $-2\overline{v_s' v_z'}\, e_{sz}$, with the strain rate $e_{sz}$ defined according to equation (11). Assuming a triangular distribution of $-\overline{v_s' v_z'}$, between 0 at the water surface and $u_*^2$ at the bottom, and assuming a logarithmic vertical profile of $v_s$, this can be elaborated to

$$-2\overline{v_s' v_z'}\, e_{sz} = \frac{1}{\kappa}\frac{u_*^3}{H}\left(\frac{H}{z}-1\right) \quad \text{or} \quad \frac{-2\overline{v_s' v_z'}\, e_{sz}}{u_*^3/H} = \frac{1}{\kappa}\left(\frac{H}{z}-1\right). \tag{16}$$

This function is shown in figure 7(*c*). The measured distribution of this component $-2\overline{v_s' v_z'}\, e_{sz}/(u_{*,60}^3/H)$ in the present experiment is shown in figure 7(*a*). In the central region, kinetic energy is transferred from turbulence to the mean flow in the part of the water column where $\partial v_s/\partial z < 0$, since $-2\overline{v_s' v_z'}\, e_{sz}/(u_{*,60}^3/H) < 0$. Considerable magnitudes of this quantity are found in this region: $-2\overline{v_s' v_z'}\, e_{sz}/(u_{*,60}^3/H) = O(-50)$. Near the bottom, mean flow kinetic energy is dissipated into turbulence, with transfer rates that strongly increase towards the bottom and reach values of $-2\overline{v_s' v_z'}\, e_{sz}/(u_{*,60}^3/H) = O(300)$. This measured order of magnitude agrees with that from the straight-flow profile in figure 7(*c*). In the part of the outer-bank region that is covered by the measuring grid, this component of the kinetic energy transfer is relatively small.

Close to the bottom, the kinetic energy transfer component $-2\overline{v_n' v_z'}\, e_{nz}/(u_{*,60}^3/H)$ (figure 6*b*) is associated with the transversal component of the bottom friction. Its maximum near-bottom values in the central region are of a similar order of magnitude to those associated with the downstream component of the bottom friction, $-2\overline{v_n' v_z'}\, e_{nz}/(u_{*,60}^3/H) = O(100)$.

In the central region, the pattern of $-2\overline{v_s' v_n'}\, e_{sn}/(u_{*,60}^3/H)$ (figure 7*b*), is similar to that of $-2\overline{v_s' v_z'}\, e_{sz}/(u_{*,60}^3/H)$ (figure 7*a*). In the upper part of the water column, where $\partial v_s / \partial z < 0$, it is negative, whereas it is positive in the lower part and strongly increases near the bottom, up to values $O(100)$. The latter was to be expected, since $-\overline{v_s' v_n'}$ represents downstream friction on the vertical projection of the inclined bottom. The strong increase of this term towards the outer bank is obviously associated with the bank friction. Yet, the turbulence production by the bank shear stress only reaches values of $-2\overline{v_s' v_n'}\, e_{sn}/(u_{*,60}^3/H) = O(20)$, which is significantly smaller than the turbulence production by the bottom shear stress. This indicates that the bank shear stress is considerably smaller than the bottom shear stress, which is in agreement with the observed smaller turbulence activity in the outer-bank region (Blanckaert & Graf 2001).
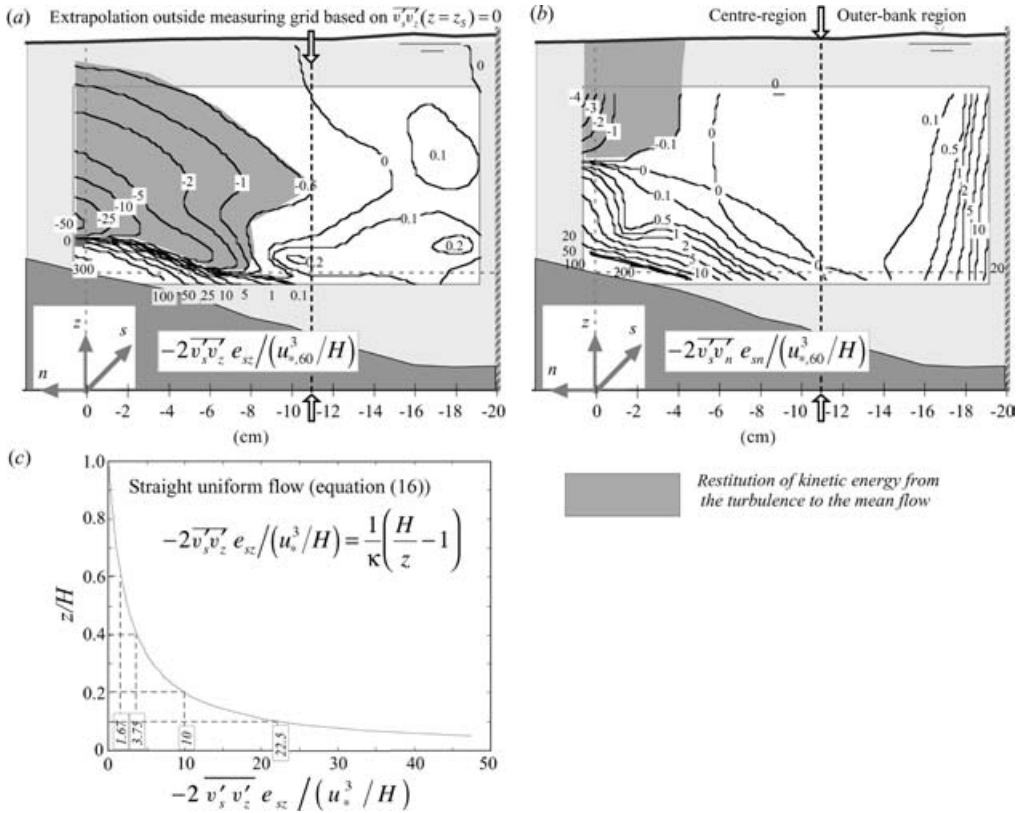
FIGURE 7. Isolines of the normalized kinetic energy fluxes between the mean flow and the turbulence via the shear stresses: $(a, b)$ experimental data for curved flow (cf. equation (9)); $(c)$ theoretical profile for straight uniform flow (cf. equation (16)).

Mean flow kinetic energy is thus mainly transferred to turbulence in the boundary layers, especially near the bottom. The normalized kinetic energy flux related to boundary friction reaches values $O(100)$. Except for $-2\overline{v_s'v_z'}\,e_{sz}/(u_{*,60}^3/H) = O(-50)$, the normalized kinetic energy fluxes in the centre region are at least one order of magnitude smaller, namely $O(1 \text{ to } 10)$, over most of the water column. In the outer-bank region outside the area dominated by the sidewall friction, they are at least another order of magnitude smaller, namely $O(0.1)$. So the kinetic energy transfer via the cross-stream turbulent stresses in the regions covered by the two circulation cells represents a negligible part of the total kinetic energy transfer between mean flow and turbulence. Hence it is irrelevant to the total energy expenditure in a bend. Nonetheless, we have shown that these small kinetic energy fluxes play an essential role in the formation of the circulation cells, hence the distribution of the downstream velocity and the boundary shear stress.

## 10. Conclusions

Previous investigations of strongly curved turbulent flow, in which only the downstream vorticity equation was considered, have not produced a clear picture of the physics leading to the co-existence of two cross-stream circulation cells. The present analysis, based on high-quality three-dimensional flow measurements in a

single cross-section of a sharp open-channel bend such as occurs in nature, considers the combination of the downstream vorticity balance and the kinetic energy transfer between mean flow and turbulence. This leads to a better physical understanding, especially of the role of turbulence. Furthermore, it gives guidance for the numerical modelling of flow in sharply curved open-channel bends.

The *centre-region cell* is dominated by the balance between the driving centrifugal term and the dissipating shear stress term in the downstream vorticity equation. Advective momentum transport by the cross-stream circulation cell decreases the downstream velocities in the upper part of the water column, while increasing them in the lower part. The strength of the centre-region cell depends on the vertical profile of the downstream velocity, which leads to a negative feedback between the downstream velocity profile and the centre-region cell, and thus to a considerably weaker centre-region cell than expected on the basis of the classical first-order perturbation approach. In the case of mild to moderate curvature, a vorticity equation simplified to the above balance is nonetheless suitable for determining the velocities in the centre-region cell, provided that it is combined with a downstream momentum equation that takes due account of the advective redistribution phenomenon.

In the case of strong curvature, when the velocity maximum is found in the lower part of the water column, this simplified model would yield two opposite centre-region cells on top of each other. The observed existence of a single centre-region cell that covers the entire water column is to be attributed to advective transport of vorticity, which compensates for the negative centrifugal term. The accurate simulation of the centre-region cell for these strong curvatures requires the use of fully three-dimensional momentum equations, including the advective transport terms.

In the outer-bank region, both the centrifugal force and the cross-stream turbulent stresses contribute to the generation of the *outer-bank cell*. Here the sign of the centrifugal term in the vorticity equation complies with the sense of rotation of the outer-bank cell, which means that the centrifugal force enhances this circulation. Terms related to the cross-stream turbulent stresses, representing the anisotropy of those stresses due to the proximity of flow boundaries, are of the same order of magnitude as the centrifugal term and mainly enhance the outer-bank cell. In the outer-bank cell, vorticity generation by the centrifugal term and by the cross-stream turbulence strengthen each other. The experimental results indicate that an outer-bank cell will also occur in the case of weak curvature, and that its occurrence is not caused by flow instability, like in the laminar flow case.

Linear turbulence closure models are unable to represent the turbulence-generated part of the outer-bank cell, although they may well produce a certain anisotropy of the cross-stream turbulence. When described with such a linear turbulence model, the cross-stream turbulent stresses always dissipate mean flow vorticity, since the kinetic energy transfer can only be from mean flow to turbulence. The experimental results indicate that kinetic energy is also transferred from turbulence to the mean flow. Although this restituted amount of kinetic energy is small compared to the total production of turbulent kinetic energy, which is mainly due to boundary friction, it plays an essential role in the dynamics of the outer-bank cell. Turbulence closures that include the possibility of kinetic energy transfer between turbulence and mean flow in either direction are therefore required to accurately reproduce the outer-bank cell.

## Appendix. Estimation of the experimental uncertainty

### A.1. *Uncertainty in the raw data*

The measured data can decomposed as

$$\tilde{f}_{raw}/f = 1 + \sigma_{raw}, \tag{A1}$$

with $\tilde{f}$ the measured value, $f$ the real value and $\sigma$ the relative uncertainty.

Rolland (1994) and Hurther (2001) estimate the uncertainty in the mean-velocity measurements by the ADVP as typically less than 4%, and the uncertainty in the turbulent normal stresses, the turbulent shear stresses and the turbulent kinetic energy as less than 10%. For the present data set, Blanckaert & Graf (2001) have made more conservative estimates for the turbulent shear stresses, $\pm\,20\%$, and for the cross-stream velocities, $\pm 0.002\,\mathrm{m\,s}^{-1}$ (which amounts to about $\pm 10\%$). These higher relative uncertainties are mainly due to the low mean values of these quantities:

$$\sigma_{raw}(v_s) < 4\%, \qquad \sigma_{raw}(v_n) \sim \sigma_{raw}(v_z) < 10\%, \tag{A2}$$

$$\sigma_{raw}(\overline{v_i'^2}) \sim \sigma_{raw}(k) < 10\%, \qquad \sigma_{raw}(\overline{v_i'v_j'}) < 20\%. \tag{A3}$$

The uncertainty in the turbulence measurements increases progressively towards the bottom, due to the steep mean-velocity gradient in the measuring volume: the lower 20% of the water column is affected by it. For that reason, the ADVP measurements focus on the outer flow region, away from the bottom.

### A.2. *Comparison with other velocimeters*

The ADVP was specially designed at EPFL (Rolland 1994; Hurther 2001) for laboratory investigations such as reported herein. Garbini, Forster & Jorgensen (1982) have reported that ADV and hot-film anemometers yield close agreement in the dynamic range of turbulence. Blanckaert & Lemmin (2004) have shown the superiority of the ADVP over commercially available ADV systems: it has a better turbulence resolution and measures simultaneously entire profiles. Lemmin & Rolland (1997) and Hurther & Lemmin (1998) have compared the ADVP to LDA and hot-film anemometers, and found comparable uncertainties in turbulence data. The ADVP has a lower temporal resolution, but a higher spatial resolution thanks to its profiling capacity. Its relatively low temporal resolution ($\sim 20\,\mathrm{Hz}$) is not a major drawback for the present work, which focuses on the interaction between the mean flow and the turbulence. In the higher frequency range, turbulence is nearly isotropic and merely dissipates energy, without dynamically interacting with the mean flow. Its higher spatial resolution makes the ADVP superior for the present purpose: it yields better-defined spatial patterns of the measured quantities and allows a more accurate evaluation of the terms in the equations for vorticity and energy transfer.

### A.3. *Uncertainty in estimation of terms in the vorticity equation and the energy transfer*

The high spatial resolution of our data allows an efficient smoothing by means of two-dimensional splines with weight functions (de Boor 1978, chaps. 14 and 17). The smoothed distribution of the variables is found as a compromise between smoothness and closeness to the raw data. Since the procedure is subjective, no hard estimation

of the uncertainty can be made. However, the smoothing efficiently eliminates the indeterminate errors, and it can reasonably be assumed that the remaining error (mainly determinate error) varies slowly in space:

$$\tilde{f}_{spline}/f = 1 + \sigma_{spline} \quad \text{with} \quad \sigma_{spline} < \sigma_{raw}. \tag{A 4}$$

The terms in the vorticity equation and the energy transfer are typically of the form $(\partial f_1/\partial y)(\partial f_2/\partial z)$, and can be decomposed according to equation (A 1) as

$$\frac{(\partial \tilde{f}_1/\partial y)(\partial \tilde{f}_2/\partial z)}{(\partial f_1/\partial y)(\partial f_2/\partial z)} = 1 + \frac{\partial \sigma_1 f_1/\partial y}{\partial f_1/\partial y} + \frac{\partial \sigma_2 f_2/\partial z}{\partial f_2/\partial z} + \left(\frac{\partial \sigma_1 f_1/\partial y}{\partial f_1/\partial y}\right)\left(\frac{\partial \sigma_2 f_2/\partial z}{\partial f_2/\partial z}\right), \tag{A 5}$$

where the last term is negligible. This is a standard result of error propagation theory, based on the worst-case assumption that the errors are cumulative.

Now, since the remaining error in the smoothed variables is assumed to vary slowly in space, it can reasonably be assumed that

$$\frac{\partial \sigma_{spline} f/\partial(y, z)}{\partial f/\partial(y, z)} < \frac{\sigma_{spline} f}{f} = \sigma_{spline} \quad \text{except where } f \text{ is close to zero}, \tag{A 6}$$

whence:

$$\frac{(\partial \tilde{f}_1/\partial y)(\partial \tilde{f}_2/\partial z)}{(\partial f_1/\partial y)(\partial f_2/\partial z)} < 1 + \sigma_1 + \sigma_2. \tag{A 7}$$

A similar expression can be derived for terms including derivatives of second order.

According to the above, the uncertainty in the evaluated terms in the vorticity equations (4)–(6) can be estimated as

$$\sigma(\omega_s) = \sigma\left(\frac{\partial v_z}{\partial n} - \frac{\partial v_n}{\partial z}\right) < \sigma(v_z) + \sigma(v_n) = 20\%, \tag{A 8a}$$

$$\sigma\left[\frac{1}{1+n/R}\frac{\partial}{\partial z}\left(\frac{v_s^2}{R}\right)\right] < 2\sigma(v_s) = 8\%, \tag{A 8b}$$

$$\sigma\left[v_n\frac{\partial \omega_s}{\partial n} + v_z\frac{\partial \omega_s}{\partial z}\right] \sim \sigma\left[v_n\frac{\partial \omega_s}{\partial n}\right] < 30\% \text{ since the second term is negligible}, \tag{A 8c}$$

$$\sigma\left[\frac{\partial^2}{\partial z\partial n}\left(\overline{v_n'^2} - \overline{v_z'^2}\right) + \frac{1}{1+n/R}\frac{1}{R}\frac{\partial \overline{v_n'^2}}{\partial z}\right] < 20\% \text{ since the last term is negligible},$$
$$\tag{A 8d}$$

$$\sigma\left[\left\{\frac{1}{1+n/R}\frac{\partial^2}{\partial z^2} - \frac{\partial}{\partial n}\left(\frac{1}{1+n/R}\frac{\partial}{\partial n}\right)\right\}[(1+n/R)\overline{v_n' v_z'}]\right] < 40\%; \tag{A 8e}$$

and the uncertainty in the evaluated energy fluxes between the mean flow and the turbulence, equation (9), as

$$\sigma\left[\left(\overline{v_i'^2} - \frac{2}{3}k\right)e_{ii}\right] < 30\%, \qquad \sigma[2\overline{v_i' v_j'}\, e_{ij}] < 40\%. \tag{A 9}$$

It should be emphasized that these estimations are rather conservative. In our analysis, we compare the relative importance of different terms in the same flow regions, as well as the relative importance of the same terms in different flow regions (centre region vs. outer-bank region). It turns out that terms are either of comparable magnitude (e.g. the centrifugal term and the cross-stream turbulence terms in the vorticity equation for the outer-bank region), or differ by at least an order of magnitude (the energy

fluxes via the cross-stream turbulence stresses, for example, are an order of magnitude smaller in the outer-bank region than in the center-region). Our interpretations are based on first-order distinctions only. Since the experimental uncertainty is always less than 40%, our results and interpretations are not corrupted by experimental inaccuracies.

## REFERENCES

ANWAR, H. O. 1986 Turbulent structure in a river bend. *J. Hydr. Engng ASCE*, **112**, 657–669.

BATCHELOR, G. K. 1970 *An Introduction to Fluid Dynamics*. Cambridge University Press.

BATHURST, J. C., THORNE, C. R. & HEY, R. D. 1979 Secondary flow and shear stress at river bends. *J. Hydr. Div. ASCE* **105**, 1277–1295.

BLANCKAERT, K. 2001 Discussion on: Bend-flow simulation using 2D depth-averaged model, by Lien H. C. *et al. J. Hydr. Engng ASCE* **127**, 167–170.

BLANCKAERT, K. 2002*a* Secondary currents measured in sharp open-channel bends. *Proc. River Flow 2002, Louvain, Belgium* (ed. D. Bousmar & Y. Zech), vol. 1, pp. 117–125. Balkema.

BLANCKAERT, K. 2002*b* Flow and turbulence in sharp open-channel bends. PhD thesis 2545, Ecole Polytechnique Fédérale Lausanne, Switzerland (available at ftp://lrhmac15/Pub/ Thesis/Blanckaert/PhD).

BLANCKAERT, K. & GRAF, W. H. 2001 Mean flow and turbulence in open-channel bend. *J. Hydr. Engng ASCE* **127**, 835–847.

BLANCKAERT, K. & GRAF, W. H. 2004 Momentum transport in sharp open-channel bends. *J. Hydr. Engng ASCE* (in press).

BLANCKAERT, K. & LEMMIN, U. 2004 Improving acoustic turbulence measurements. Submitted for publication. (Also chapter I.2 in Blanckaert (2002*b*).)

BLANCKAERT, K. & DE VRIEND, H. J. 2004 Non-linear modeling of mean flow redistribution in curved open channels. *Water Resour. Res.* (in press).

BOOIJ, R. 2003 Measurements and large eddy simulations of the flows in some curved flumes. *J. Turbulence* **4**, 1–17.

BOOIJ, R. & TUKKER, J. 1996 3-Dimensional laser-Doppler measurements in a curved flume. In *Proc. 8th Intl Symp. on Developments in Laser Techniques and Applications to Fluid Mechanics*, Lisbon, pp. 98–114. Springer.

DE BOOR, C. 1978 *A Practical Guide to Splines*. Springer.

BOUSSINESQ, J. 1868 Mémoire sur l'influence de frottement dans les mouvements réguliers des fluides; XII – Essai sur le mouvement permanent d'un liquide dans un canal horizontal à axe circulaire. *J. Math. Pures Appl.* (2) **XIII**, 413.

BRADSHAW, P. 1987 Turbulent secondary flows. *Annu. Rev. Fluid Mech.* **19**, 53–74.

BRUNDETT, E. & BAINES, W. D. 1964 The production and diffusion of vorticity in duct flow. *J. Fluid Mech.* **19**, 375–394.

CHENG, K. C., LIN, R.-C. & OU, J.-W. 1976 Fully developed laminar flow in curved rectangular channels. *Trans. ASME: J. Fluids Engng* **98**, 41–48.

CHOUDHARY, U. K. & NARASIMHAN, S. 1977 Flow in 180° open channel rigid boundary bends. *J. Hydr. Div. ASCE* **103**, 651–657.

CHRISTENSEN, B., GISLASON, K. & FREDSOE, J. 1999 Secondary turbulent flow in an infinite bend. *1st RCEM Symp., Genova, Italy*, vol. 1, pp. 543–553. University of Genova.

COLOMBINI, M. 1993 Turbulence-driven secondary flows and formation of sand ridges. *J. Fluid Mech.* **254**, 701–719.

DEMUREN, A. O. & RODI, W. 1984 Calculation of turbulence-driven secondary motion in non-circular ducts. *J. Fluid Mech.* **140**, 189–222.

DIETRICH, W. E. 1987 Mechanics of flow and sediment transport in river bends. In *River Channels: Environment and Process* (ed. K. Richards), pp. 179–227. Inst. Brit. Geog. Special Publication, Oxford.

DIETRICH, W. E. & SMITH, J. D. 1983 Influence of the point bar on flow through curved channels. *Water Resourc. Res.* **19**, 1173–1192.

EINSTEIN, H. A. & HARDER, J. A. 1954 Velocity distribution and the boundary layer at channel bends. *Trans. AGU* **35**, 114–120.

EINSTEIN, H. A. & LI, H. 1958 Secondary currents in straight channels. *Trans. AGU* **39**, 1085–1088.

ENGELUND, F. 1974 Flow and bed topography in channel bends. *J. Hydr. Div. ASCE* **100**, 1631–1648.

FALCON ASCANIO, M. & KENNEDY, J. F. 1983 Flow in alluvial-river curves. *J. Fluid Mech.* **133**, 1–16.

GARBINI, J. L., FORSTER, F. K. & JORGENSEN, J. E. 1982 Measurements of fluid turbulence based on pulsed ultrasound techniques. Part 2. Experimental investigation. *J. Fluid Mech.* **118**, 471–505.

GESSNER, F. B. 1973 The origin of secondary flow in turbulent flow along a corner. *J. Fluid Mech.* **58**, 1–25.

GESSNER, F. B. & JONES, J. B. 1965 On some aspects of fully developed turbulent flow in a rectangular channel. *J. Fluid Mech.* **23**, 689–713.

GÖTZ, W. 1975 Sekundärstromungen in aufeinander folgenden Gerinnekrümmungen. *Mitteilungen* 163. Theodor-Rehbock Flussbaulaboratorium, Karlsruhe.

HILLE, P., VEHRENKAMP, R. & SCHULZ-DUBOIS, E. O. 1985 The development and structure of primary and secondary flow in a curved square duct. *J. Fluid Mech.* **151**, 219–241.

HINZE, J. O. 1975 *Turbulence*. McGraw-Hill.

HURTHER, D. 2001 3-D acoustic Doppler velocimetry and turbulence in open-channel flow. PhD thesis 2395, Ecole Polytechnique Fédérale Lausanne, Switzerland.

HURTHER, D. & LEMMIN, U. 1998 A constant beamwidth transducer for three-dimensional Doppler profile measurements in open channel flow. *Meas. Sci. Technol.* **9**, 1706–1714.

HURTHER, D. & LEMMIN, U. 2001 A correction method for turbulence measurements with a 3-D acoustic Doppler velocity profiler. *J. Atmos. Ocean. Technol.* **18**, 446–458.

IKEDA, S., YAMASAKA, M. & KENNEDY, J. F. 1990 Three-dimensional fully developed shallow-water flow in mildly curved bends. *Fluid Dyn. Res.* **6**, 155–173.

JIA, Y., BLANCKAERT, K. & WANG, S. S. Y. 2001 Numerical simulation of secondary currents in curved channels. *Proc. 8th Intl Symp. on Flow Modelling and Turbulence Measurements, Tokyo* (ed. A. Wada, H. Ninokata & N. Tanaka). World Scientific.

JOHANNESSON, H. & PARKER, G. 1989 Secondary flow in mildly sinuous channel. *J. Hydr. Engng ASCE* **115**, 289–308.

KALKWIJK, J. P. TH. & DE VRIEND, H. J. 1980 Computation of the flow in shallow river bends. *J. Hydr. Res. IAHR* **18**, 327–342.

KAWAHARA, Y. & TAMAI, N. 1988 Note on turbulence modelling for secondary flows in passages of non-circular cross-section. *Proc. Japanese Soc. Civ. Engng* **399**/II-10, 247–250 (in Japanese).

KIKKAWA, H., IKEDA, S. & KITAGAWA, A. 1976 Flow and bed topography in curved open channels. *J. Hydr. Div. ASCE* **102**, 1327–1342.

LEMMIN, U. & ROLLAND, T. 1997 Acoustic velocity profiler for laboratory and field studies. *J. Hydr. Engng* **123**, 1089–1098.

MOCKMORE, C. A. 1943 Flow around bends in stable channels. *Trans. ASCE* **109**, 593–628 (incl. discussions).

NAOT, D. & RODI, W. 1982 Calculation of secondary currents in channel flow. *J. Hydr. Div. ASCE* **108**, 948–968.

NEZU, I. & NAKAGAWA, H. 1984 Cellular secondary currents in straight conduits. *J. Hydr. Engng ASCE* **110**, 173–193.

NEZU, I. & NAKAGAWA, H. 1993 *Turbulence in Open-Channel Flows*. IAHR-Monograph, Balkema.

NEZU, I., NAKAGAWA, H. & TOMINAGA, A. 1985 Secondary currents in a straight channel flow and the relation to its aspect ratio. In *Turbulent Shear Flows 4* (ed. L. J. S. Bradbury *et al.*), pp. 246–260. Springer.

NEZU, I. & NAKAYAMA, T. 1998 Mutual-interaction between bursts and boils very near the free-surface of open-channel flows. In *Environmental Hydraulics* (ed. J. H. L. Lee *et al.*), pp. 297–303. Balkema.

NEZU, I. & NAKAYAMA, T. 1999 Numerical calculation of steep open-channel flows by considering effects of surface-wave fluctuations. In *Hydraulic Modelling* (ed. V. P. Singh *et al.*), pp. 3–16. Water Resources Publications, Colorado.

ODGAARD, A. J. 1984 Bank erosion contribution to stream sediment load. *IIHR Rep.* 280. Iowa Institute of Hydraulic Research, Iowa.

PERKINS, H. J. 1970 The formation of streamwise vorticity in turbulent flow. *J. Fluid Mech.* **44**, 721–740.

PRANDTL, L. 1942 *Führer durch die Strömungslehre*. Vieweg, Braunschweig.

ROLLAND T. 1994 Développement d'une instrumentation Doppler ultrasonore: application aux écoulements turbulents en hydraulique. PhD thesis 1281, Ecole Polytechnique Fédérale Lausanne, Switzerland.

ROZOVSKII, I. L. 1957 *Flow of Water in Bends of Open Channels.* Acad. Sci. Ukraine SSR; Israeli Prog. Sci. Transl., Jerusalem, 1961.

SCHLICHTING, H. & GERSTEN, K. 2000 *Boundary-Layer Theory*, 8th Edn. Springer.

SHIONO, K. & MUTO, Y. 1998 Complex flow mechanisms in compound meandering channels with overbank flow. *J. Fluid Mech.* **376**, 221–261.

SIEBERT, W. 1982 Strömungscharakteristiken in einem Kanal mit 180°-Krümmungen. *Mitteilungen* 168. Theodor-Rehbock Flussbaulaboratorium, Karlsruhe.

SPEZIALE, C. G. 1987 On nonlinear $K$–$l$ and $K$–$\varepsilon$ models of turbulence. *J. Fluid Mech.* **178**, 459–475.

THOMSON, W. 1876 On the origin of windings of rivers in alluvial plains, with remarks on the flow of water round bends in pipes. *Proc. R. Soc. Lond.* **25**, 5–8.

TOMINAGA, A., EZAKI, K., NEZU, I. & NAKAGAWA, H. 1989 Three-dimensional turbulent structure in straight channel flows. *J. Hydr. Res. IAHR* **27**, 149–173.

TOMINAGA, A., NAGAO, M. & NEZU, I. 1999 Flow structure and momentum transport processes in curved open-channels with vegetation. *28th IAHR Congr., Graz, Austria.* Institute for Hydraulics and Hydrology, Technical University, Graz.

DE VRIEND, H. J. 1977 A mathematical model of steady flow in curved shallow channels. *J. Hydr. Res. IAHR* **15**, 37–54.

DE VRIEND, H. J. 1981a Steady flow in shallow channel bends. *Rep.* 81-3, Lab. Fluid Mech., Dept. Civil Engng, Delft University of Technology.

DE VRIEND, H. J. 1981b Velocity redistribution in curved rectangular channels. *J. Fluid Mech.* **107**, 423–439.

DE VRIEND, H. J. & GELDOF, H. J. 1983 Main flow velocity in short and sharply curved river bends. *Rep.* 83-6, Lab. Fluid Mech., Dept. Civil Engng, Delft University of Technology.

WINTERS, K. H. 1987 A bifurcation study of laminar flow in a curved tube of rectangular cross-section. *J. Fluid Mech.* **180**, 343–369.